UNIVERSIDADE DO ALGARVE
FACULDADE DE CIÊNCIAS E TECNOLOGIA

Electrical characterization of electronic interfaces to communicate with electrogenic cells *in vitro*

Pedro Miguel Cavaco Carrilho dos Santos Inácio

Dissertação para obtenção do Grau Mestre em

Engenharia Eletrónica e de Telecomunicações

Orientador: Prof. Doutor Henrique Leonel Gomes (Universidade do Algarve)
Coorientadora: Prof.ª Doutora Maria do Carmo Medeiros (Universidade de Coimbra)

Setembro 2013

Electrical characterization of electronic interfaces to communicate with electrogenic cells *in vitro*

Pedro Miguel Cavaco Carrilho dos Santos Inácio

Dissertação para obtenção do Grau Mestre em

Engenharia Eletrónica e de Telecomunicações

Setembro 2013

Electrical characterization of electronic interfaces to communicate with electrogenic cells *in vitro*

"Declaração de autoria de trabalho"

Declaro ser o autor deste trabalho, que é original e inédito. Autores e trabalhos consultados estão devidamente citados no texto e constam da listagem de referências incluída.

Pedro Miguel Cavaco Carrilho dos Santos Inácio

À Margarida,

Aos meus Pais

À minha Família.

Agradecimentos

A realização deste trabalho no âmbito da dissertação para obtenção do grau de Mestre em Engenharia Eletrónica e Telecomunicações constitui para mim uma honra, uma vez que me tem permitido aplicar os conhecimentos e competências, que adquiri nas várias disciplinas do Mestrado, enquanto desenvolvo um trabalho de investigação inserido no âmbito de um consórcio europeu, o *iOne-FP7*. Quero assim expressar o meu agradecimento ao meu orientador, Professor Doutor Henrique Leonel Gomes, pelo apoio, pela oportunidade e pelo convite para participar neste projeto, bem como por todo o acompanhamento e incentivo que sempre me tem transmitido; agradeço igualmente à Professora Doutora Maria do Carmo Medeiros, coorientadora neste trabalho, por toda a preciosa ajuda que facultou, pelo seu rigor e profissionalismo.

Agradeço ainda a todos aqueles que me têm acompanhado e que de alguma forma têm contribuído, quer na construção do meu conhecimento quer na minha formação como pessoa e profissional – aos meus colegas neste trabalho e a todos os professores nele envolvidos, pela amizade, apoio logístico e discussões; à Universidade do Algarve, aos técnicos e funcionários que, de alguma forma, deram o seu contributo para a construção dos dispositivos utilizados.

Quero ainda agradecer à Margarida pelo seu Amor, Doação, e Compromisso de partilha - obrigado pela dedicação em que eu me sinta sempre um homem feliz e realizado, e pela sua constante presença na minha vida! Agradeço também aos meus Pais, por terem sido incondicionalmente um alicerce firme na minha vida, transmitindo-me sempre a confiança e apoio nos melhores e piores momentos e decisões da minha vida - obrigado pelo vosso Amor, Carinho, e Compromisso. Por último, agradeço à minha Família, que me ajudou a crescer e a tornar-me na pessoa que sou, partilhando muitos bons momentos da vida.

Acknowledgments

The accomplishment of this dissertation for the degree of Master of Engineering Electronics and Telecommunications is an honor for me, since it has allowed me to apply the knowledge and skills that I acquired in the various disciplines of the Master, while developing a research inserted within a European consortium, the *iOne-FP7*. So I want to express my gratitude to my advisor, Professor Henrique Leonel Gomes, for the support, the opportunity and the invitation to participate in this project, as well as all the monitoring and encouragement that he has always transmitted; I am also grateful to Professor Maria do Carmo Medeiros, co-adviser in this work, all the precious help she has provided for his thoroughness and professionalism.

I am also grateful to those who have accompanied me and who somehow have contributed in the construction of my knowledge and in my training as a person and professional - my colleagues in this work and all the teachers involved in it, the friendship, logistical support and discussions; to the University of the Algarve, the technicians and staff who, somehow, have contributed to the construction of the devices used.

I would also like to thank Margarida for her love and commitment - thanks for the dedication that makes me feel always a happy and fulfilled man, and its constant presence in my life! I also thank my parents, for being unconditionally a firm foundation in my life, always passing me the trust and support in the best and worst moments and decisions of my life - thank you for your love, affection, and commitment. Finally, I thank my family, who helped me to grow and become the person I am, sharing many good moments of life.

Resumo

O presente documento reflete o trabalho realizado no âmbito do desenvolvimento de novos materiais eletrónicos biocompatíveis e biodegradáveis que veio permitir a construção de transístores implantáveis em seres vivos e capazes de comunicar com células nervosas (neurónios). Estes componentes eletrónicos serão capazes de reparar partes do tecido nervoso e restaurar a comunicação entre tecidos nervosos, por exemplo reparar lesões na medula espinal.

A motivação deste trabalho surge com a necessidade de desenvolver novos instrumentos que nos ajudam a perceber aspetos fundamentais da biologia, nomeadamente sobre como as células nervosas interatuam umas com as outras e respondem a estímulos elétricos e bioquímicos. Para tal, foi efetuada uma pesquisa que envolve vários aspetos, (i) a aplicação de materiais biocompatíveis com propriedades elétricas para a construção de transístores, (ii) estudo de processos eletroquímicos que ocorrem na interface entre o transdutor e a membrana celular, e (iii) a aquisição e estímulo de sinais bioelétricos.

No decorrer da investigação, foram caracterizados componentes eletrónicos capazes de operar em meios eletrolíticos complexos, nomeadamente, condensadores do tipo Metal-Isolador-Semicondutor (MIS); foram realizadas técnicas de medidas de ruído elétrico e análise espectral para a identificação de sinais bioelétricos, bem como foram obtidos e caracterizados os sinais bioelétricos produzidos por células quando submetidas a estímulos elétricos e bioquímicos extracelulares. Estas técnicas de medidas vêm comprovar a possibilidade de monitorizar a adesão das células e o seu estado de saúde, a sua atividade bioelétrica e o efeito provocado pela adição de estímulos extracelulares.

Palavras-chave: Biossensores; Bio eletrónica; Neuro-eletrónica; Biotransístor; técnicas de diagnóstico.

Abstract

This document reflects the work done in the development of new electronic biocompatible and biodegradable materials that allow the construction of implantable transistors in living beings, able to communicate with nerve cells (neurons). These electronic components will be able to repair parts of the nervous tissue and restore communication between the nerve tissues, e.g. repair spinal cord injury.

The motivation of this work arises from the need to develop new instruments that help us understand fundamental aspects of biology, in particular on how nerve cells interact with each other and respond to electrical and biochemical stimuli. For this purpose, a search was performed involving various aspects, (i) applying biocompatible materials with electrical properties for constructing transistors, (ii) the study of electrochemical processes occurring at the interface between the transducer and the cell membrane, and (iii) acquisition and stimulation of bioelectric signals.

During investigation were characterized electronic components capable of operating in complex electrolyte media, in particular, capacitors of the type Metal-Insulator-Semiconductor (MIS); electrical noise measurement techniques and spectral analysis for identifying bioelectrical signals were carried out, and were obtained and characterized the bioelectric signals produced by cells when subjected to electrical and extracellular biochemical stimulation. These technical measures prove the possibility to monitor the cells adhesion and their health state, their bioelectric activity and the effect caused by the addition of extracellular stimuli.

Keywords: Biosensors; Bioelectronics; Neuro-electronics; Biotransistor; diagnostic techniques.

Index

Index of figure

Index of Tables

Abbreviations

DL	Double-Layer
ECPs	Electrically Conducting Polymers
EDL	Electrical Double Layer
EIS	Electrolyte-Insulator-Substrate
FETs	Field-Effect Transistors
GPIB	General Purpose Interface Bus
ICS	Intelligent Cell Surfaces
IHP	Inner Helmholtz Plane
iONE-FP7	Implantable Organic Nano-Electronic – Seventh Framework Programme
MEAs	Microelectrode Arrays
MGSs	Micro Gold-Spines
MIS	Metal-Insulator-Semiconductor
NTs	Nanotubes
NWFETs	Nanowire Field-Effect Transistors
NWs	Nanowires
O-CSTs	Organic Cell Stimulating and sensing Transistors
OECTs	Organic Electrochemical Transistors
OFETs	Organic Field-Effect Transistors
OHP	Outer Helmholtz Plane
OSCs	Organic Semiconductors
OTFTs	Organic Thin-Film-Transistors
PDCH	Petri Dish and Chip Holder
PSD	Power Spectrum Density
SWNTs	Single-Wall Nanotubes
USB	Universal Serial Bus

Chapter 1

INTRODUCTION

There are several pathologies that have lack of means to achieve its cure and / or better understanding. Hence raises the need to investigate the utility that micro and nano electronics technology can offer to biomedicine.

The root of this idea was born in 1780, the University of Bologna, when Luigi Galvani conducted a series of experiments that led the way for bio electrogenesis, relating the use of bioelectric forces with tissues of living organisms [1].

In [2], the author makes the analogy between computers and brains, noting that the common factor between them is working electrically; however, also notes that the large difference in mobility of ions in a solid structure of silica (about 10^3 cm^2/Vs) and an aqueous structure (about 10^{-3} cm^2/Vs) is the reason for the different operation of the architecture of the two information processors.

Thus, since the idea generated by L. Galvani, new horizons have arisen in research, looking for the development of an electrogenic interface. However, such knowledge generates knowledge, with the passage of time, new issues appear, in particular with regard to which material should be used to build such devices capable of implementing said electrogenic interface.

This work aims to characterize devices able to operate in complex electrolytic means. Thus, future research may find a solution to solve the complex problem presented earlier, the junction between the "brain" and "processor".

The idea of this project is based on the following key concepts: bioelectric interface, biocompatible implants electronic, acquisition and stimulation of biological signals.

1.1 Motivation and Objectives

The modern electronic displays today miniaturization of high quality; there are being developed nanometric devices that derive from organic and inorganic matter. Considering the fact that the growing demand for new ways of learning and research of biological media, from professionals in the biomedical area through the use of electronic equipment, there is a need and reason to develop electronic components capable of operating in complex electrolytic means, i.e., required to implement an interface between the biological environment and the computational means.

In order to achieve the development of an eletrogenic interface, were pre-determined the following objectives:

- Characterization of electronic components capable of operating in complex electrolytic medium;
- Performing measurements of electrical noise and spectral analysis for the identification of bioelectric signals;
- Collection and characterization of bioelectric signals produced by cells when subjected to electrical and biochemical stimulus.

Another motivating factor is the fact that this project is inserted in a European consortium, the *iOne-FP7*, and the project intelligent cell surfaces (*ICS*) financed by Portuguese foundation for science and technology.

1.2 Contributions

The main contributions of this project are:

- Developed of sensing devices in collaboration with Philips®.
- Devices and knowledge imparted by the various partners of the European project *iONE-FP7* and *ICS*.
- Collection of a library of bioelectrical signals from cells in vitro.

1.3 Structure of the Thesis

This work is divided into 6 parts:

- The first consists of the introduction and Chapter 2, where it is reviewed the literature to support the development of this study (State of Art);
- Chapter 3 presents and develop holder able to support different electronic devices sensing devices with cell cultures in vitro;
- Chapter 4 presents the experimental set-up to record cells bioelectrical activity;
- In chapter 5 presents the results and the respective critical analysis
- Finally, in Chapter 6, are identified conclusions and perspectives for future work to keep developing this project.

Chapter 2

STATE OF THE ART

In this chapter literature that supports this research is reviewed.

2.1 BIOELECTRONICS

Modern electronics started in 1947 with the appearance of the first transistor built based on inorganic semiconductors by Bardeen, Brattain and Shockley. In 1958, Jack Kirby built the first device with an integrated electronic circuit based on planar technology on a substrate of germanium [3], emerging as the way of the current micro- and nanoelectronics. Later, in 1977 Shirakawa, MacDiarmid and Heeger developed the first organic semiconductor materials, the *polyacetylene* [4].

Recently based on advanced microelectronic devices, new ideas have emerged for application of electronic devices in biological media, such as suggested in [2], the analogy between the brain and a processor.

Thus began the generation of bioelectronics, based on two fronts, the devices based on organic and inorganic matter. Earlier, bioelectronic devices began to be studied to operate in different ways: in a first configuration, presupposed the monitoring of the devices performance in terms of potential, impedance, resistance, charge transport, among others, working as a support to knowledge effects in biological media devices while trying to figure out how to interact with biological media; in a second configuration, attempted to design bioelectronic devices for required functions, such as the biosensors [5].

However, the junction between the two configurations mentioned above determines the ultimate goal of bioelectronics, i.e, implementing an electrogenic interface capable of operating in complex biological media. This is also the focus of many research groups, working on developing electrogenic interfaces based on inorganic and organic materials.

2.2 BIOELECTRIC DEVICES

The raw metal electrodes that are typically used in active implantable devices are often associated to a poor stimulation and recording performance in the long term [27].

It is thus important the concern in developing bioelectrical devices that are biocompatible while maintaining good performance in the long term. For this purpose, the key is to use inorganic and organic matter as solutions for insulators and semiconductors.

Thus, this 2.2 point will be divided into two: the first shows the electrical devices developed based on inorganic matter, and the second, the devices developed based on organic matter.

2.2.1 INORGANIC DEVICES

Silicon (Si) is commonly used as a substrate for three reasons: (i) being an electrical conductor, which can be isolated with very thin layers of silicon dioxide (SiO_2) thickness ranging from 10 to 1000nm, thus making the silicon in a inert substrate perfect for cell culture, (ii) silicon dioxide suppress the transfer of electrons and prevent the electrochemical process leading to the etching of silicon, (iii) it is a technology well implemented in the marketplace, with high quality in microelectronics [2].

For these reasons, research groups have developed devices based on the same technology, are mostly devices based in transistors *FET-EIS* (*Electrolyte-Insulator-Semiconductor*) [6].

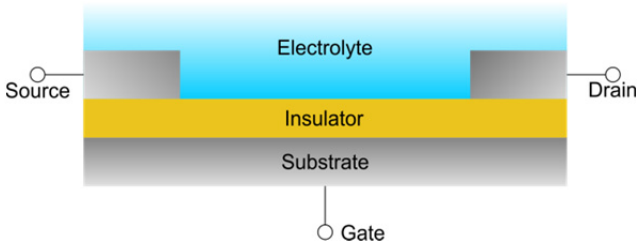

Fig. 1 – Physical structure of a transistor *FET-EIS*.

In Fig. 1, **Substrate** is the semiconductor substrate layer (typically Si); **Insulator** is the insulating layer (typically SiO_2) with varying thickness; **Electrolyte** is the "layer" that surrounds the device (cells culture medium), constituting the channel of the transistor; **Source** and **Drain** are the electrodes (usually, are metals: gold (Au) or platinum (Pt)).

These electronic devices implement interfaces to cells, however are limited to functions as: sensibility to extracellular ion flow using *ion-sensitive FET* (*ISFET*) [2], acquisition of electrical and chemical signals [7], cell stimulation [8], cell adhesion [9] and [10], detection of cellular metabolism [11], among others.

Recently, new devices have been developed using nanotechnology such as *nanowire FETs* (*NWFET*) together with *Nanotube* (*NT*), verifying whether they have excellent performance in respect of predecessors *FET* transistors, with an average increase of transconductance from 45 to 800 nS, and an average increase of mobility from 30 to 560 cm^2 / V.s [12].

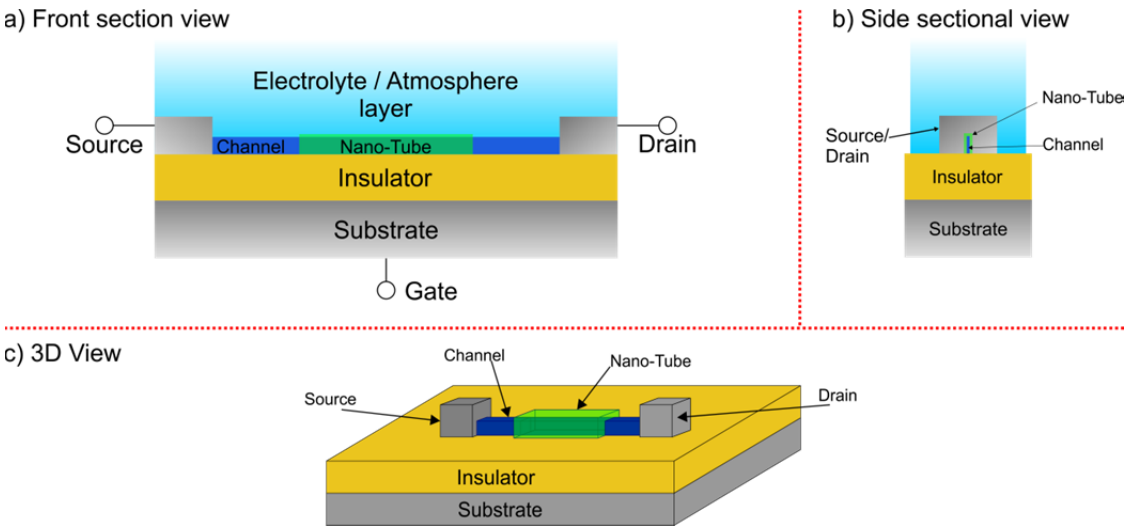

Fig. 2 – Physical structure of NWFET-*NT*.

In Fig. 2, **Source** and **Drain** correspond to electrodes that lie on the insulator layer; in (a) **Channel** represents a nano layer between the electrodes, and (b) a layer which is much narrower than the electrodes; **Nano-Tube** is isolation between the channel layer and *Electrolyte* layer, which may it covers the entire channel or just part of it.

Several research works with devices that are based on the principles of *NT-NWFET* have been made for the application of nanotechnology to bioelectronics, as is the case of the application devices composed by *NWs's arrays* for acquisition of biomolecular signal [13], or *single-wall nanotubes* (*SWNT*) devices for the acquisition of bioelectric signals [14].

In [15], there is an application of *NWFET-NT* that proves that the improvements in the acquisition of bioelectric signals, in relation to those previously obtained with *FET-EIS* devices. These improvements are due to the replacement of traditional metal contacts (electrodes) wide and flat (with hundreds of μm^2), for electrodes with *micro-spines (MGS)*, running these as tiny "needles" in which cells will become settled.

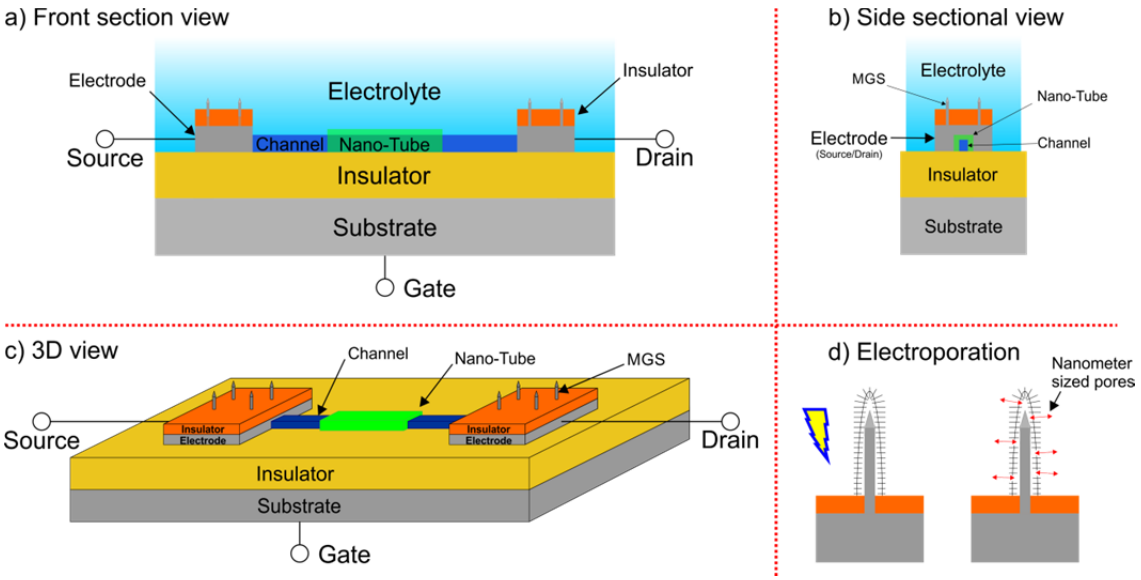

Fig. 3 – Physical structure of *NWFET-NT-MGS*.

In Fig. 3, it appears that the devices *NWFET-NT-MGS* have a physical structure similar to those mentioned in Fig. 1; however it is observed in (a) and (b) that electrodes of *MGS-NT-NWFET* are constituted by two layers, a conductive layer (the electrode) made of Pt, and another layer on the electrode which is insulator and made of silicon nitride (Si_3N_4), verifying that the *MGS* are physically connected to the electrode, crossing perpendicularly the insulator layer. In (d), in a reduced scale, occurs the electroporation process that the MGS induce in cell membranes after a few cycles of polarization and hyperpolarization of the cell. In [15], is a study of cell behaviour in the presence of *microelectrode arrays* (*MEAs*).

However, devices with structures like those shown previously in Fig. 1, Fig. 2 and Fig. 3 wherein the substrates are Si and the insulating layer is an oxide (SiO_2), are more likely to contain defects, but also are extremely sensitive to alkali ions that often lead to oxide ruptures or hysteresis of devices [17], and is therefore very important the search for fusion devices based on organic matter (which will be presented below in section 2.2.2) and those presented at this point 2.2.1 [18].

2.2.2 ORGANIC BASED TRANSISTORES

The conductors / semiconductors based on organic matter (conductive polymers) have been the focus of attention by many researchers since its discovery in 1977. Since then, there have been developed new polymers with conductive properties and various

applications in electronics today, among them *Polyaniline* (PANI), *Poly(ethylenedioxythiophene)* (PEDOT), *Poly(phenylene vinylidene)* (PPV), *Poly(dialkylfluorene)* (PDAF), *Poly(thiophene)* (PTs) and *Poly(pyrrole)* (PPy) [4]. In 1984 (Wrighton *et al.*, 1984 cit. in [18]) developed the first transistor using organic material, an *organic electrochemical transistor* (*OECT*), thus initiating the new era of organic electronics.

The biggest advantages that organic devices present, compared to inorganic devices, come from low production costs through the use of printing techniques [19] and [20], as well as the ability to adjust the organic material properties for the intended purpose [18], while allowing the conjugation of polymers with substances such as drugs [1].

However, with the application of organic material to the bioelectrical devices, arises the problem of biocompatibility *versus* biodegradability [28], since the suitability of organic materials greatly differs, depending on the way they are synthesized and the overall nature of system conjugation with the substrate polymer, or its chemical composition, surface charge distribution and acidy [1].

Given these limitations it has been found that among various polymers, the PEDOT doped *poly(styrenesulfonate)* (PSS) forms a composition (PEDOT: PSS), which the quality of adhesion from cell culture closely resembles what happens in glass slides [1] such as seen by the investigation that explores the quality of the interaction from PEDOT with cell cultures *in vitro* [21].

In this study we performed a cell culture on an electrode, and after the accession of them, PEDOT was deposited in the saline solution (electrolyte medium), which already contained PSS and was involving the culture; this process is called electropolymerization.

In Fig. 4 is shown a device based on electropolymerization, demonstrating the simplicity and functionality of the electrical interaction between PEDOT and cells.

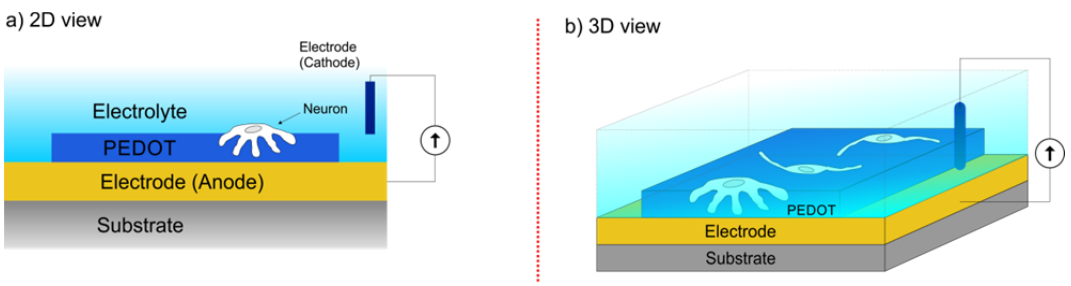

Fig. 4 – Physical structure of the device based on electro polymerization [21].

Also in [21] is referred that electropolymerization may become a future solution for fixing cells to an electrode; more recent studies [22] have confirmed that the creation of PPy or PEDOT nanotubes on electrodes promotes adhesion and cell proliferation.

In [18] is a summary of various organic devices capable of operating in complex electrolytic medium which served as a base for the first interfaces with cells *in vitro*, such as: organic electrochemical transistor (*OECT*) ([29], [30] and [30]), organic transistor FET (*OFET*) ([17] and [23]), *ion-sensitive* transistor *OFET* (*ISOFET*) [34] and *electrolyte-gated* transistor *OFET* (*EGOFET*) ([35] [36]).

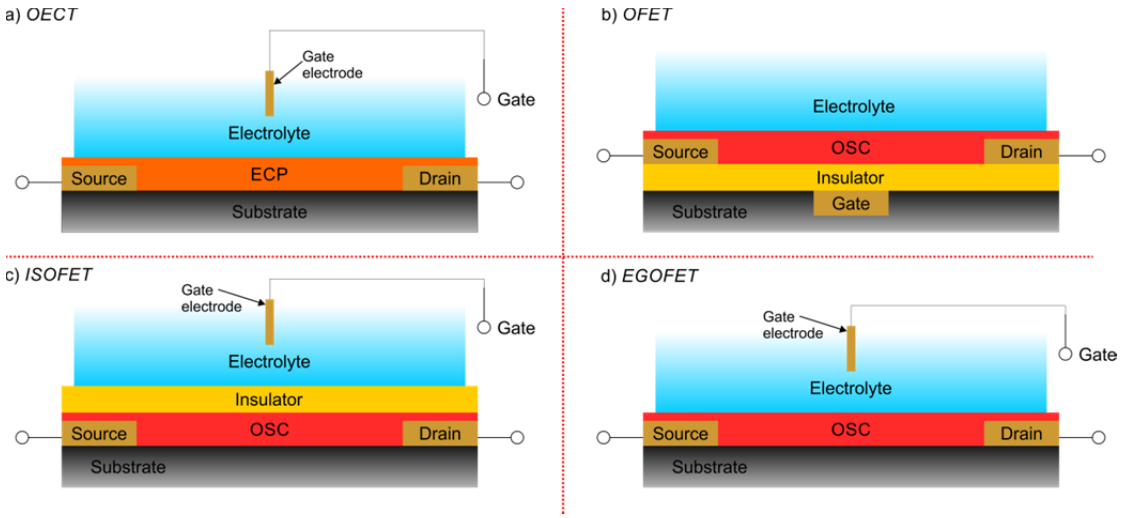

Fig. 5 – Physical structure of the device *OECT*.

Fig. 5 shows in (a) the physical structure of a *OECT*, being the operating principle based on the interaction of the conducting polymer layer (*electrically conducting polymer* - ECP) with electrolytic medium and cells.

Source and **Drain** terminals are merely representative and both are constituted by the *ECP*; differentiation in color comes from the possibility of existence of links with different metals to make connection to measurement instruments.

The gate terminal is introduced into the electrolytic medium intending to make changes in the conductivity of the *ECP*'s layer through the application of electric stimuli that lead to doping or non-doping the polymer. Recent studies found that an electrolytic medium containing PSS, or in the case of PEDOT being doped with PSS, it is not necessary to stimulate conjugation PEDOT: PSS with the *Gate* so that there is conductivity. Thus the *OECTs* become ionic current converters into electric current, and therefore may be considered excellent displays of biological phenomena [18] and [34].

In (b) is shown the physical structure of an *OFET*, and its working principle is very similar to the *FET-EIS's* presented in paragraph 2.2.1, differing only in the layer of organic semiconductor (*OSC*) which lies on the *insulator* layer.

The *OSC* layer eases the production of *FET* devices, allowing design devices with different dielectric properties related to the combination *OSC-insulator* [18].

In (c) is shown the physical structure of an *ISFET*; these devices are adapted to explore the charges polarization, using the *insulator* layer in direct contact with the surrounding electrolyte medium.

Thus, using a *top Gate*, electrical potential may be induced on the *OSC* layer, i.e. current is modeled in *Drain* through the polarization of the charges in the *OSB* [18] and [34].

Finally, in (d) is shown the physical structure of an *EGOFET*, which the operating principle is based on the effect produced by the electrical double layer (*EDL*) formed by interfaces *OSC-electrolyte* and *electrolyte-Gate*.

Depending on the *Gate*'s polarization, ions are distributed to opposite interfaces, allowing current modulation in the *Drain* composed by *OSC* layer [18].

2.3 BIOELECTRIC SIGNALS

All biological systems are regulated by a multiplicity of electrical signals, and these assure the regulation of each cell functions and control the function of multicellular systems such as tissues and vital organs.

Inside an organism, these signals can be "transported" via either blood vessels or along neurons; in this case, the information transmission from one neuron to another is made by signals passing through the synaptic cleft [1].

The cell, the basic unit of any living tissue, presents an anatomy and physiology appropriate to her role. All cells present, along their membrane structure, a potential difference which is a difference in electric charge resulting from uneven load distribution between the region immediately adjacent to the interior and exterior of the cell membrane [33]; in the case of nerve cells, these are electrically excitable, which means that a stimulus produces a series of characteristic changes in resting potential, and their membranes can produce and conduct electrochemical impulses [33].

According to [18], is believed that the potential difference of the cell membrane responsible for producing and conducting electrochemical impulses is very important for the correct functioning of the cell.

The origin of said potential difference is in the excitement of the nerve cell, which in turn will generate the aforementioned pulse, also called bioelectrical signal, which will then propagate [18].

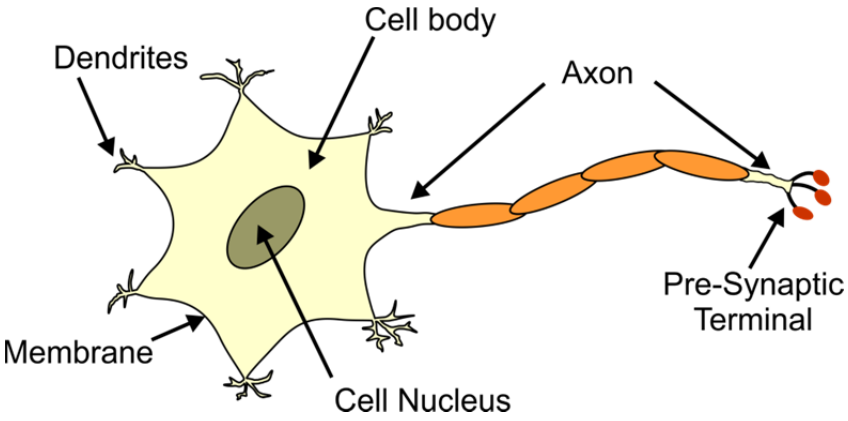

Fig. 6 – Simplified structure of a neuron.

In general, it can be said that a nerve cell is composed of four physiological units: dendrites, cell body, axon and presynaptic terminals.

Dendrites receive impulses from other cells, leading them to the cell body (structure where are the nucleus and other organelles); these impulses can be excitatory or inhibitory. The axon receives the bioelectric signal (pulse) from the cell body and transfers it to the next cell via pre-synaptic terminals ([26] and [32]).

The communication between neurons and from these to other tissues in the body is made via electrical signals called *action potentials*. These signals consist of brief, invariant and large electrical impulses and result from the application of a stimulus at a given point in the cell leading to depolarization, which reaches a designated by *threshold level*, in the membrane cell. The action potential is a major change in membrane potential that propagates without changing its amplitude, across the cell membrane ([32] and [33]).

Action potentials are all-or-none signals. This means that if stimulus provided to the cell is below a certain threshold, there's no action potential production; if, on the contrary, the stimulus provided is above the said threshold, an electrical signal is generated always with constant amplitude. Action potentials propagate along an axon at a speed of up to 150 m/s without decaying [32].

At rest no current flows through the cell membrane. The neuron becomes excited when a local change in membrane potential occurs. If this change is above the threshold mentioned above, the neuron "fires" action potentials [32].

The number of action potentials is determined by the amplitude and duration of the input stimulus. So information transmitting is frequency-coded. Input stimuli can be received either from other neurons through the dendrites or by a direct physical or chemical stimulation, e.g. olfactory sensory neurons [32].

The neuron membrane is formed by a double layer of lipid molecules, and presents hydrophobic properties. Due to the chemical properties of these molecules, there is a separation of electrical charges across the membrane, which gives rise to differences in electrical potential transversely in the membrane; this is called the *membrane potential* [26].

2.4 ELECTRIC NOISE IN A CELL MEMBRANE

The possible effects that electromagnetic radiation emitted by high voltage power lines have on human health have been subject of discussion for some time now. Power frequencies of high voltage lines are low enough to interfere with cell membranes, which are highly resistant; thus, researchers have developed studies to assess the effect that the electric field induces in the membrane cells, comparing it with the proper electrical noise generated by the Brownian motion of the membrane.

Human exposure to electric fields is not new: since the dawn of human evolution, man has already been exposing himself to a slowly fluctuating field of about 100 V/m as he is moving around objects. However, with the high-voltage lines, the situation is different: almost all over the world there are giant metal structures that support a vast network of high voltage power lines that can carry up to half a million volts. When standing right under a power line a person can be exposed to about 10kV/m [37].

Many data have been gathered, analyzed, and reanalyzed over the last quarter century in order to understand the possible effects that exposure to these fields can cause to human health in the long term, but epidemiological studies have been somewhat inconclusive. The epidemiological inconclusiveness all the more justifies a biophysical approach: where and how does an electric field interact with a living

organism? Can we come up with some thresholds that have to be exceeded before a physiological effect can occur? [37]

Electromagnetic radiation has an electric and a magnetic component; following, the approach will be taken regarding possible physiological effects resulting from the electric component [37].

Living cells, by virtue of the underlying molecular processes, ion channel movements and dipole oscillations, exhibit intrinsic electric currents. (These currents have magnitudes on the order of a few femto to pico-amperes (10^{-15} to 10^{-12}). The measurements of these currents reveal valuable knowledge of underlying biochemical, physiological and pathological processes [37].

The intracellular and extracellular medium is very ionic and conducts well. So when an electric field is imposed on a piece of living tissue, the ions move and, within a microsecond, compensate for the field inside the liquid [37].

The cell membrane is very resistive and this means that, once a steady state is reached, the entire voltage drop occurs across the cell membranes [37].

The significance of an added nanovolt-order ELF oscillation across a cell membrane was first approached with rigorous quantitative physics in 1990 by Weaver and Astumian (WA) [37].

2.4.1 THERMAL NOISE IN A CELL MEMBRANE

Because of the Brownian motion of the charge carriers, there is always a small fluctuating voltage between the two ends of a resistor. This voltage was first measured and explained in 1928 by Johnson-Nyquist (JN). The so-called Johnson-Nyquist (JN) noise is white and in a frequency window of the average square voltage is expressed as:

$$\langle \Delta \boldsymbol{V^2} \rangle = \boldsymbol{4 k_B T R (\Delta f)} \quad (1)$$

where k_B is the Boltzman constant $\left(1.3806488 \times 10^{-23} (\mathrm{J/K^{-1}})\right)$, T is the absolute temperature, R is the resistance and Δf the bandwidth.

For noise analysis, the cell membrane can be conceived of as a resistor.

The interfaces of the membrane with the intracellular and extracellular fluid effectively act like capacitor plates that are 5nm apart. In the WA view the

transmembrane noise can be evaluated as the noise between the capacitor plates in an RC parallel circuit (Fig. 7).

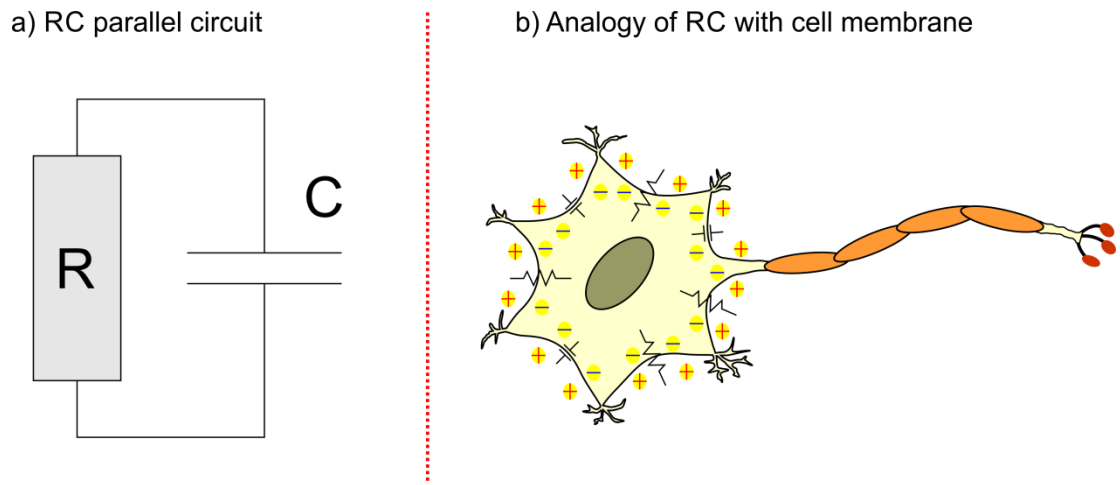

Fig. 7 – RC parallel circuit analogy with cell membrane.

In our context the resistor (R) is also a white noise generator that follows Eq. (1).

Because of the sheet-like nature of the membrane, the resistor R should then actually be conceived of as N parallel resistors that each has a resistance NR, where N is a very large number [37].

In 2002, W.T. Kaune put forward that, as a membrane protein is embedded in the cell membrane, it should, in the context of Fig. 7, be imagined to be inside the resistor [37].

Inside the resistor a protein should be subject to the electric field that presumably cause the JN-voltage of Eq. (1). Moving the protein from between the capacitor plates to inside the resistor in Fig. 7 effectively inverts the WA picture. This means that at low frequencies the field inside the resistor gets balanced out by the counter voltage from the capacitor. At high frequency the capacitor cannot follow. So eventually the protein will only “feel” the fast oscillations with periods below the RC time. In such a model, there would be a possibility for the power frequency radiation to be “stick out” above the noise spectrum [37].

2.4.2 INTRAMEMBRANAR NOISE

A cellular membrane has a thickness of approximately 5 nm, and many billions of square nanometers of surface area; so compared to that shown in Fig. 7, the resistor represented is, in fact, a very thin sheet. Considering the small conductivity of a membrane, the sheet should be modeled as an array of many parallel resistors. Taking, in that case, N parallel resistors of resistance NR leads to the same net resistance R. The amount of noise, however, increases very fast with N, and not only does the number of "noise making resistors" increase when N is increased, the amount of noise per resistor also grows with N as each individual resistors generates a voltage that follows Eq. 2.

$$\langle \Delta V^2 \rangle = 4k_B TNR(\Delta f) \tag{2}$$

At each frequency the oscillations have random phase differences relative to each other. This being out of phase leads to the resistors pushing and pulling current in and out of each other. The capacitor is not involved in this "pulling and pushing" of current, which current constitutes the intramembranous noise. The intramembranous noise increases with N and for large N, the effect of the capacitor becomes increasingly more negligible [37].

An exact mathematical solution for a value of N was first formulated by Vincze, Szasz, and Sazasz (Vincze, Szasz, and Sazasz, 2005, *cit in* [37]). A simpler derivation of the same result is found in [37]. When cutting up the membrane into the aforementioned individual resistors, a logical choice is taking the elementary resistor as a cube of 5nm x 5nm x 5nm. For an ordinary cell, this leads to a value of N of the order of millions. The noise that a membrane protein "feels" in this case is almost all intramembrane, it is many times larger than what WA would predict, and the spectrum is effectively white [37].

2.4.3 THE MEMBRANE AS A BARRIER TO IONS

As mentioned before, a cellular membrane is the most part, a lipid bilayer with no mobile charges inside. The transmembrane voltage emerges because of penetrations of the membrane by ions from the aqueous solution on either side of the membrane. These penetrations are random, and left-to-right penetrations are not necessarily balanced out by right-to-left penetrations [37].

A real membrane is also a capacitor, so any charge imbalance leads to a finite ΔV and a force, proportional to ΔV, that drives ΔV back to zero. This leads to an Ornstein–Uhlenbeck process (i.e. a random walk in a parabolic potential). These ions are not fixed at one position on the membrane-liquid interface, they move over the surface with a speed that can be estimated from $1/2\, mv^2 \approx k_B T$, and comes out to be between 10^2 and 10^3 m/s [37].

2.4.4 THE MEMBRANE AS A WHITE NOISE GENERATOR

The dimensions that we took before for an elementary resistor (5nm × 5nm × 5nm) are also realistic for a membrane protein. Whenever an ion, on its trajectory on the membrane, crosses over such a protein, the protein feels a delta function-like electric pulse. Given the 3 ions per square micrometer (μ^2) and the speed of these ions, the noise intensity that a membrane protein is subjected to due to the membrane-parallel random trajectories can be evaluated (Bier, 2005, *cit in* [37]). This noise comes out to be many orders of magnitude larger that the noise intensity due to the membrane transverse penetrations [37].

Transmembrane voltage fluctuations due to 2-sided shot noise at equilibrium were given by Eq. (1). This leads to a current power spectral density of (DeFelice, 1981, *cit in* [37]).

$$\boldsymbol{S_I^{eq} = 4k_B T/R} \tag{3}$$

The current power spectral density gives the mean square current per unit of bandwidth (i.e. Hz). The noise power in a certain frequency window is obtained by multiplying the power spectral density with the resistance and integration over the frequency window. The intensity of equilibrium noise is generally taken to be frequency independent. This "white noise" assumption is reasonable when working in a sub-MHz regime. (Bier, 2005 and DeFelice, 1981, *cit in* [37])

2.4.5 NON-EQUILIBRIUM SITUATIONS (SHOT NOISE)

For a living cell there is a continuous cycling of ions across the membrane as shown in Fig. 8. For each type of ion at steady state the same current *I* go in-to-out as well as out-to-in. In a living cell maintains electric currents across its membrane. Pumps drive ions against the electrochemical potential and channels let ions flow back. Transport through pumps "is" active and one-by-one. Channels let about 10^4 ions pass during an average channel opening. The randomness of the channel openings is the main contributor to non-equilibrium noise [37].

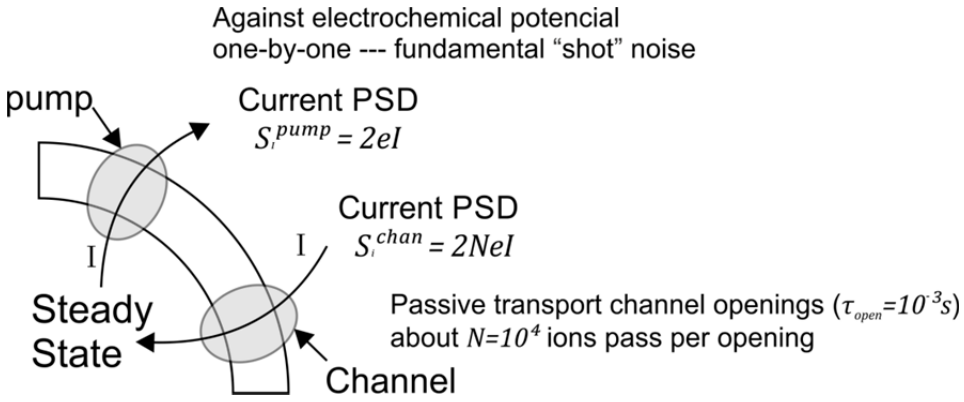

Fig. 8 – Pumps and channel of cell membrane structure.

Pumps drive ions through the membrane against the electrochemical gradient. This active transport requires energy and is commonly powered by the hydrolysis of ATP. Ion channels allow ions to flow with the electrochemical gradient. Pumps transport ions one-by-one. When the actual membrane passage time of an ion is negligible compared to the time between subsequent passages, we can think of these passages as delta function-like pulses. We then face ordinary shot noise [37].

The noise is white and the current power spectral density is easily evaluated as (DeFelice, 1981, *cit in* [37]):

$$\boldsymbol{S_I^{pump} = 2eI} \tag{4}$$

Here $\boldsymbol{I}$ represent the current and $\boldsymbol{e}$ is the elementary charge [37].

For a channel the equivalent of the pump's elementary charge is the amount of charge that passes during a channel opening. For a sodium channel, for instance, the average channel open time is about $\tau_{open} = 10^{-3}s$. The current that flows during an average channel opening is of picoampere magnitude. A picoampere current

corresponds to about 10^7 elementary charges per second. So during an average channel opening about $N = 10^4$ ions flow [37].

The current power spectral density due to channel activity is given by

$$S_I^{chan} \approx 4NeI \tag{5}$$

There is a prefactor 4 instead of a prefactor 2 because the open time of a millisecond is an average of an exponential distribution [37].

2.4.6 CHANNEL NOISE *VS* PUMP NOISE

Channel noise is larger than the pump noise by a factor of about ten thousand. This is basically because pumps transport charge in larger units. So we have $S^{noneq} \approx S^{chan}$.

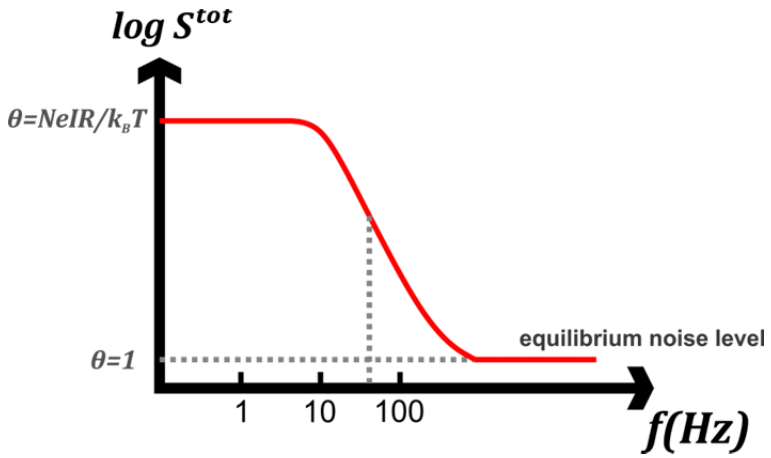

Fig. 9 – Channel noise *vs.* Pumps noise.

In Fig. 9, the measured power spectral density of noise across a cell membrane behaves like $1/f$ between about 10 Hz and about 10^4 Hz. Above 10^4 Hz the level of the white equilibrium noise starts to exceed the non-equilibrium noise. The measured plateau where f is smaller than about 10 Hz corresponds well with our estimate from Eq. (7). At the power frequencies the non-equilibrium noise is about 100 times as intense as the equilibrium noise [37].

$$S_I^{noneq} \approx 4NeI \tag{6}$$

Eq. (6) is a valid approximation as long as one looks at frequencies smaller than the channel's inverse average open time. At frequencies higher than $1/\tau_{open}$, the correlations on time scales shorter than τ_{open} make for a smaller noise amplitude. When one type of channel is involved, the eventual spectrum $S_I^{noneq}(\omega)$ is a sigmoid; a so-

called Lorentzian spectrum that drops down from $4NeI$ to zero at about $\omega = 1/\tau_{open}$ [37].

2.4.7 THE POWER SPECTRAL DENSITY OF CELL MEMBRANES

The power spectral density of actual cell membranes was first recorded in the 1960s by Verveen and Derksen (Verveen, 1966 and Derksen, 1965, *cit in* [37]). More accurate recordings have been made since (Diba, Lester and Koch, 2004 *cit in* [37]). The equation depicts the general shape of such spectra:

$$\boldsymbol{\theta = \frac{S^{noneq}}{S^{eq}} \approx \frac{4NeI}{4k_BT/R} = N\frac{e}{k_BT}IR} \tag{7}$$

The plateau that runs from zero Hz to somewhere between 1 and 10 Hz represents the level $S_I^{noneq} \approx 4NeI$ that we just calculated. Verveen and Derksen already noticed that this level was many times larger than what just equilibrium noise would predict. For the dimensionless ratio between non-equilibrium and equilibrium noise we derive as given in the equation [37].

For the current power spectral density of the equilibrium noise we ignore the intramembrane noise and took the WA estimate. Substituting realistic values for the resistance of a cell membrane we find for θ a value of about 1000. To the right of the plateau the power spectral density drops off roughly like $1/\omega$. The apparent $1/f$-noise can be explained by the fact that, in a real cell membrane, there are many types of channels with different τ_{open}'s and different ensuing values of N. The $1/f$ pattern can thus emerge as a superposition of a number of Lorentzians. It has been argued that channels may exhibit $1/f$ noise in and of themselves (Bassingthwaighte, 1994, *cit in* [37]), but these ideas are still controversial.

At the power frequency we still have a ratio S^{noneq}/S^{eq} of about one hundred.

Experimental observations affirm this (Derksen and Verveen, 1966; Diba, Lester and Koch, 2004 *cit in* [37]). As the S^{eq} according to the WA model already overwhelms the possible response to a 10 kV/m signal from a power line, including the non-equilibrium noise in the description only renders ambient ELF radiation more inconsequential [37].

2.4.8 NOISE IN NERVE CELLS

Some non-equilibrium noise may not just be noise, but actually a signal. This is most obvious with a signal going through a nerve cell. In that case a signal propagates as the opening of sodium channels triggers the opening of nearby sodium channels. These channel openings are regulated and they no longer constitute noise, but, instead, make up a signal that moves information [37].

With non-equilibrium noise in living systems we face a gray area between signal and noise [37].

Chapter 3

PETRI DISH AND CHIP HOLDER DEVICE

In this chapter, will be described a sensing device, designed by me in collaboration with members of the team involved in this project, capable to perform electronic measurements in biological environmental *in vitro*.

3.1 Features

- Transparent and biocompatible device capable to perform advanced measurements in biological environments.

- Uses of standard size Petri Dish produced by *SARSTEDT*® [1]:
  - Resistance up to $80ºC$
  - Made from transparent *polystyrene*
  - Dimension of $35x10mm$, gamma-sterile proper for ventilation cam with $5ml$ of working volume

- Uses of standard O-ring standard sizes and biocompatible[2].

- Metal screws with $16mm$ length and $2mm$ diameter, combined with adapted nuts in order to perform strength between top and bottom bases.

- Metallic gold (Au) plated pins, to perform instrument and device connection.

- Device chassis made in extrude acrylic, resistant up to $70°C$ for long period of use, and electrical characteristics: dielectric constant (ε_r) at 50Hz about 3.7, volume resistivity of $10^{15}(\Omega.cm)$ and surface resistivity of $10^{14}(\Omega)$ [3].

[1] http://www.sarstedt.com, available at 23/07/2013.
[2] http://www.prepol.com/, available at 23/07/2013.
[3] http://www.dagol.pt/uk/, available at 23/07/2013.

3.2 Description

The device Petri Dish and Chip Holder (PDCH) are general propose devices to perform cells culture *in vitro* in the top of electronic sensing devices, capable to contain 5ml of working volume approximately, and operate in biological environment as so incubator environment, where $O_2 + CO_2$ atmosphere is about $37°C$.

That device is designed exclusively for Philips® electronic devices (chip), but can be redesigned for others. The reason is to perform a Chip Holder (CH) with the correct dimensions.

3.3 PDCH Setup

The PDCH consists of the follow parts presented at Fig. 10.

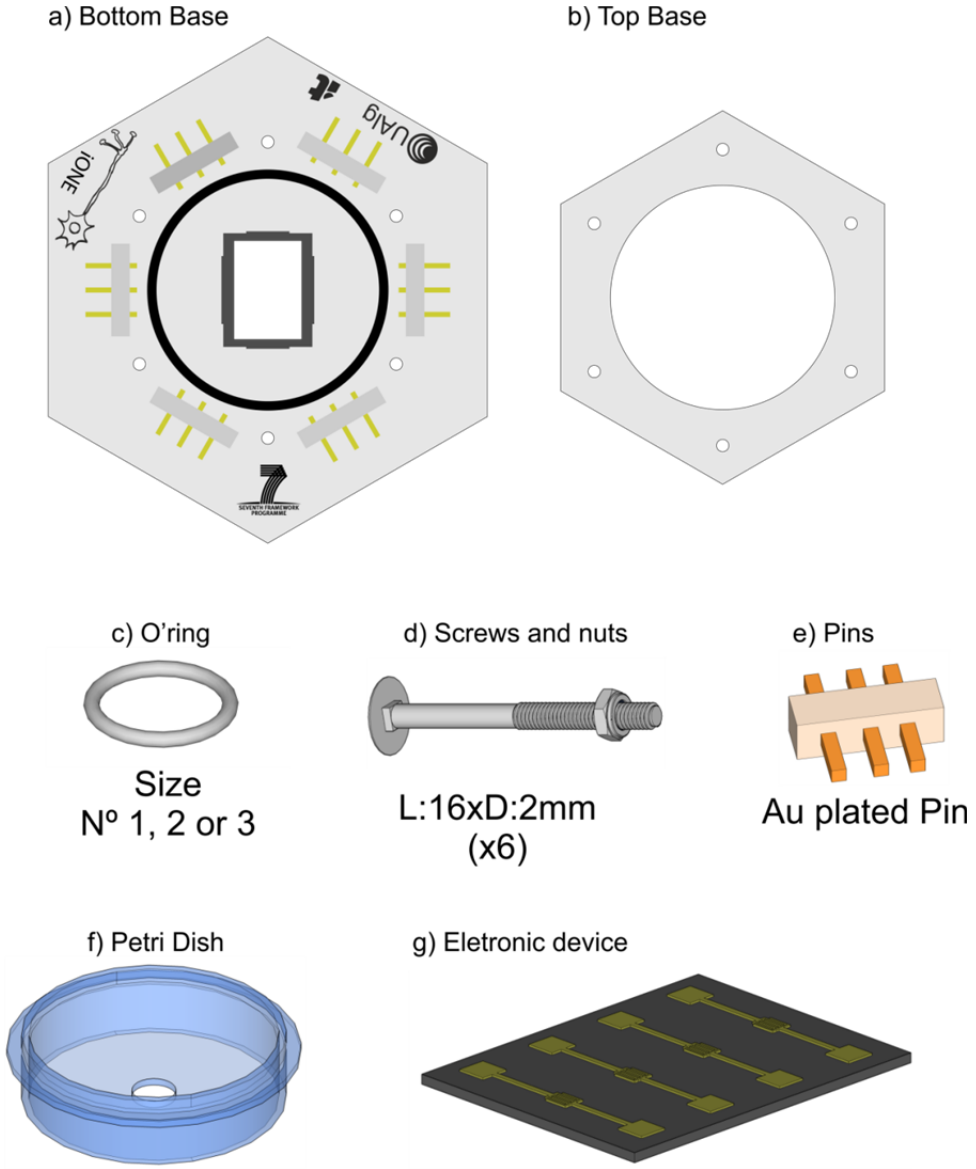

Fig. 10 – PDCH parts.

The followed scheme presented at Fig. 11, shows the different steps to assemble the sample holder with the sensing device. During the second process, it is needed to be done bindings between the device pads and the CH pins.

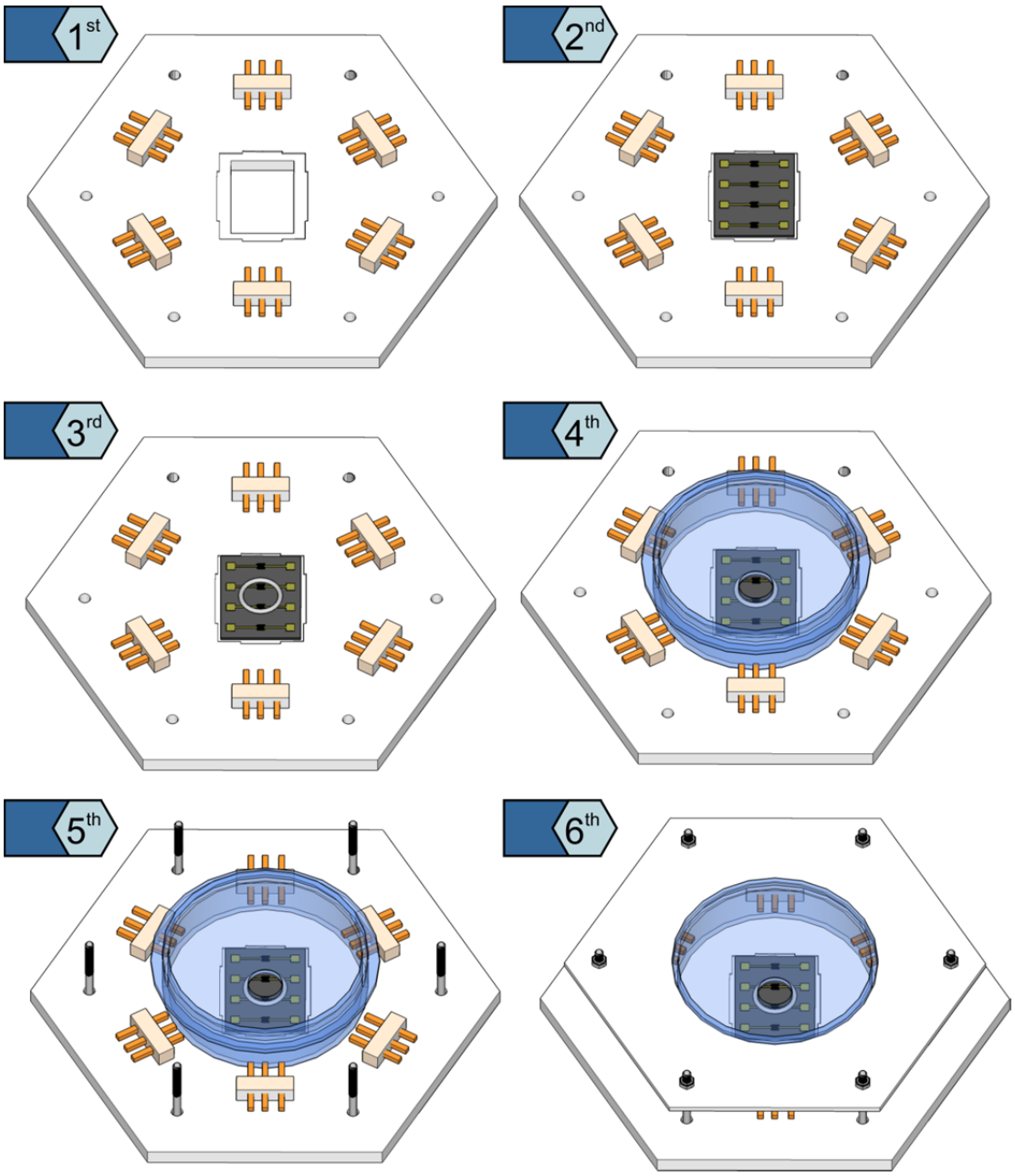

Fig. 11 – Schematic description of the steps needed to build the PDCH.

3.4 Dimensions

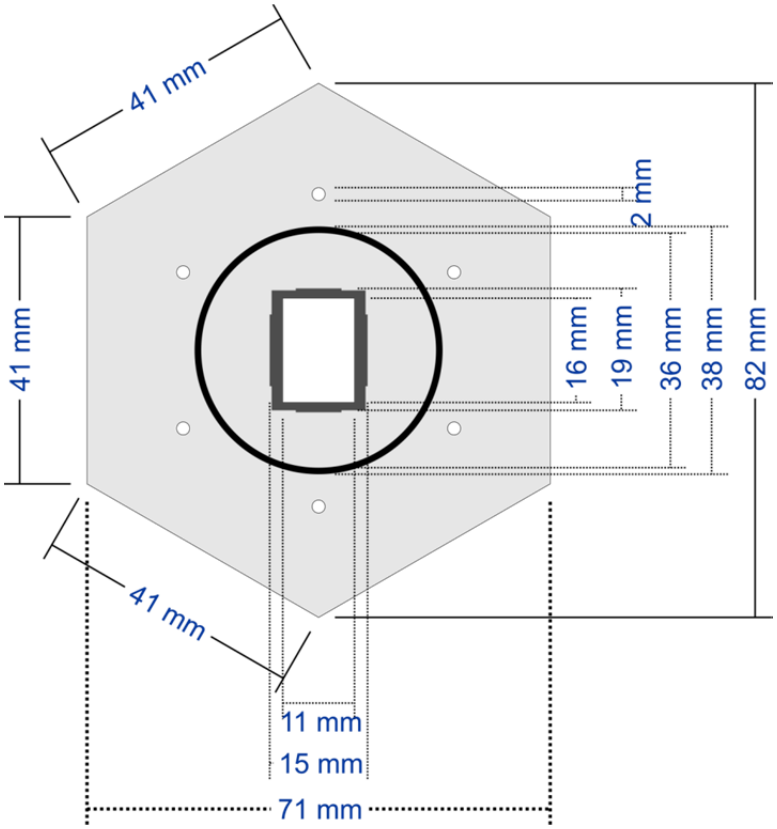

Fig. 12 – PDCH bottom base dimensions.

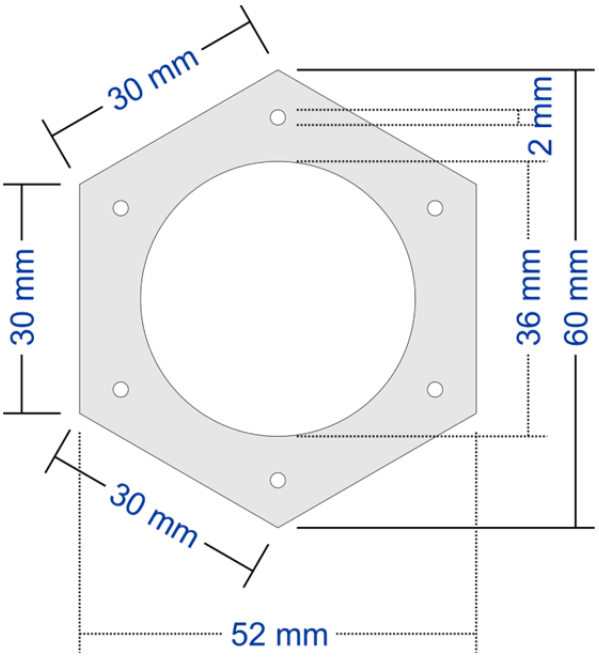

Fig. 13 – PDCH top base dimensions.

3.5 Final version release

The final prototype built of PDCH (see Fig. 14), was fabricated with transparent extruded acrylic. The Fig. 11 shows the different steps to assemble the PDCH.

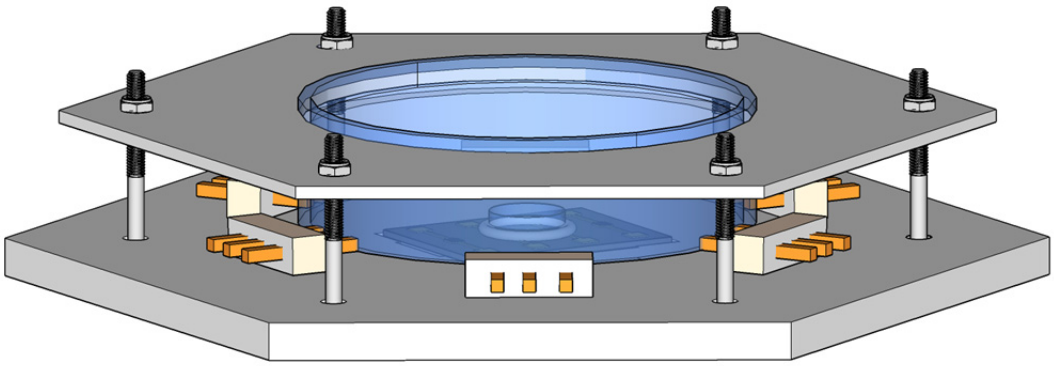

Fig. 14 – Schematics of a Petri Dish and Chip Holder (PDCH).

Chapter 4

EXPERIMENTAL SET-UP FOR ELECTRICAL MEASUREMENTS

The experimental set-up and the electronic instrumentation used to record electrical bioactivity of the cells *in vitro* are described in this chapter. The type of cells used is also briefly described.

4.1 EXPERIMENTAL SET-UP

To record the bioelectrical signals a noise measuring system was used [25]. A schematic diagram is shown in Fig. 16.

This system is comprised by an *Agilent 35670A Dynamic Signal Analyzer*, which operates together with a battery operated low-noise current pre-amplifier *Stanford Research SR570*. A *Keithley 487 picoammeter* with accuracy of 10fA and a *Keithley 2182A digital nanovoltmeter and low voltage meter* were also used to measured signals in a slow time scale. The entire measuring system together with the CO_2 incubator was placed in an iron shield with a dedicated electrical ground. The entire system is designed to eliminate parasitic interferences, particularly those caused by the 50 Hz main line.

Impedance measurements were carried out by a RCL meter a Fluke PM6306 Programmable Automatic RLC meter, with capabilities to measure Capacitance (**C**), Resistance (**R**) and Inductance (**L**), within the range of 10 Hz to 1 MHz.

Electrical stimulation of the cells in vitro was carried out by an *Agilent* 33220A *Function / Arbitrary Waveform Generator*.

The sensing devices are metal-insulator semiconductor field effect transistors (MISFETs) where the transistor channel is left empty. The living cells will fill the transistor channel. Fig. 15 shows a schematic diagram of a sensing device together with a photograph. The devices are comprised of gold microelectrode arrays spaced 10 microns (L=10 μm) and with a channel width (W) of 10.000 μm. The electrodes are on top of thermal oxidized silicon wafers. The oxide (SiO_2) is 200 nm thick and the substrate is a highly doped silicon wafer (resistance of $1 - 3\ \Omega.cm$). The oxide layer is used to couple AC signals to the junction SiO_2/membrane.

In case of chemical stimuli, the method adopted in the laboratory was to add extracellular solutions such as: Calcium Chloride Dehydrate($CaCl_2.2H_2O$), Potassium Chloride (KCl) and Dopamine.

In some cases, in order to verify that the signals measured were generated by cells and not artifacts, a neurotoxin was added to the cell culture, tetrodotoxin (TTX), which inhibits cells from producing action potential.

It is mandatory condition that a culture medium of cells *in vitro* has a sterile atmosphere and levels of oxygen (O_2), carbon dioxide (CO_2) and moisture controlled to specific values.

Thus, all the experiments were performed inside of an incubator (*Thermo Scientific Midi 40 Small Capacity CO_2 Incubator, 120*) that guarantees the maintaining of sterilization and controlled atmosphere to carry out the experiments.

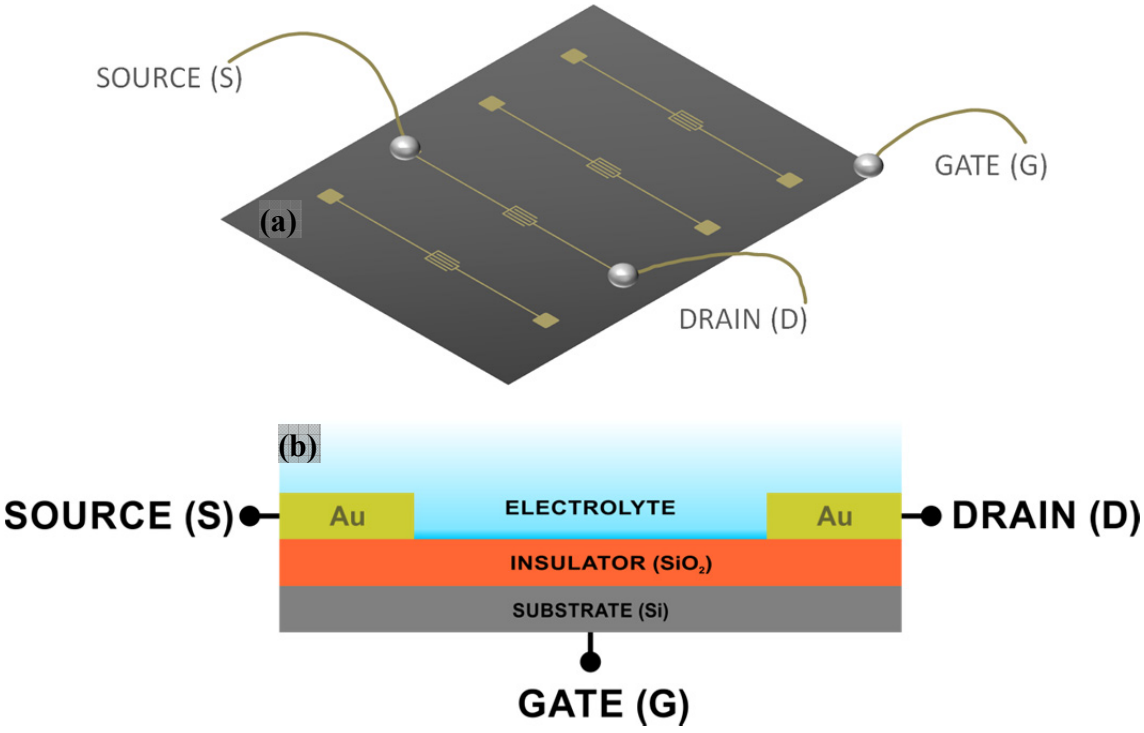

Fig. 15– (a) Photograph and (b) schematic diagram of a sensing device.

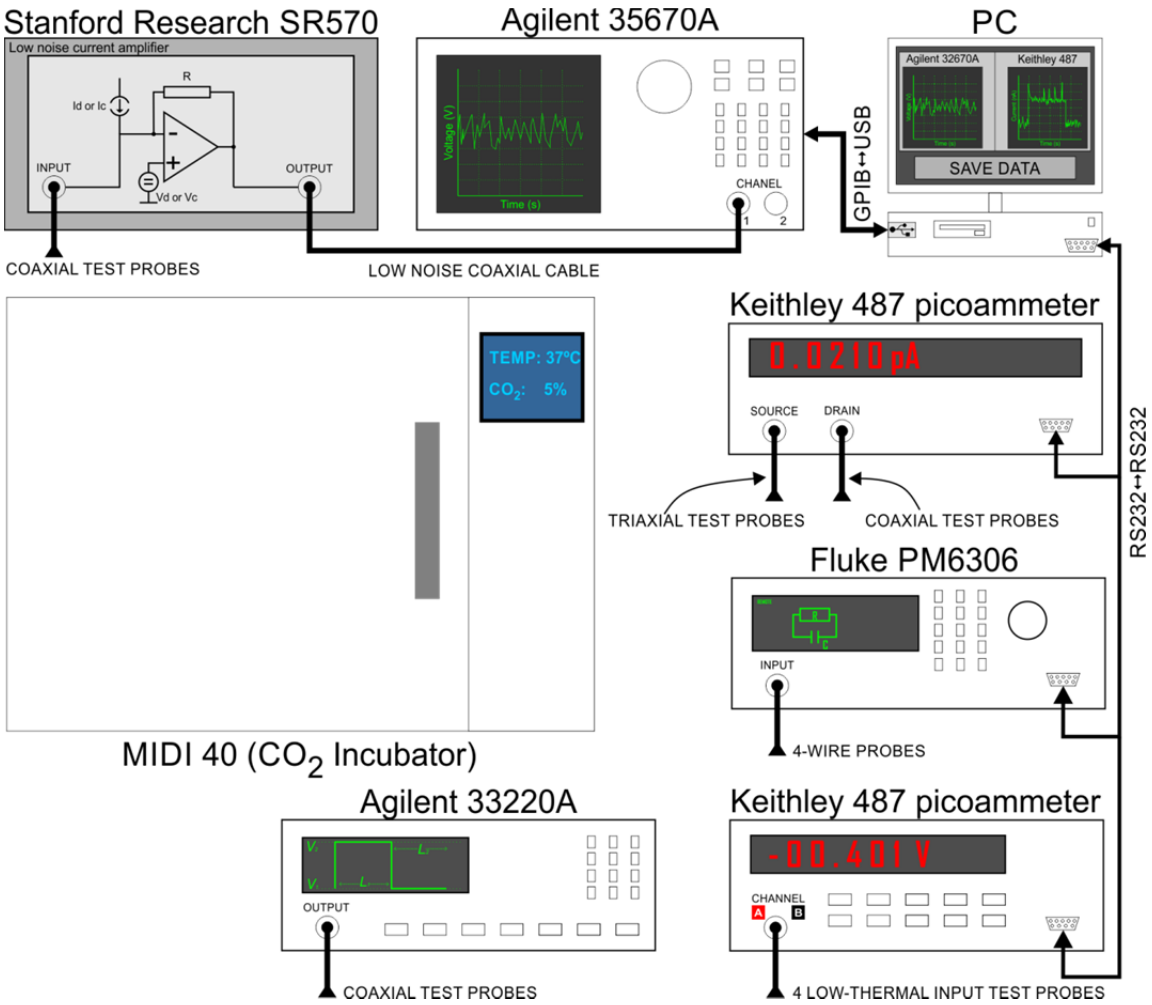

Fig. 16 – Experimental configuration of the laboratory.

In Fig. 16, it can be seen that all the measurement equipment have test leads loose, that should connect to the interface cable for the inside of incubator, in order to perform measurements.

4.2 DATA ACQUISITION PROGRAM

In order to provide better and efficient measurements, a program was developed to operate with the *Agilent 35670A Dynamic Signal Analyzer*. Fig. 17 is an illustration of the program main window. The interface used to connect instrument with the computer is GPIB-USB. Drivers are available at Agilent[4] web site which is required to control the instrument. This program has the capability to extract and reconstruct the entire frequency spectrum using different time windows. This instrument is designed to

[4] http://www.home.agilent.com/, available at 17/09/2013.

support 1, 2 or 4-channels, but the developed program only make uses of 1-channel in order to achieve a larger frequency span. The full range is from $122\mu Hz$ to $102.4\ kHz$. The frequency range can be set to automatic or manual, and the resolution lines (number of samples) per time window can be set to be within the range of 100, 200, 400, 800 or 1600 samples. By default, the instrument and the program uses automatic frequency mode (see Table I for automatic frequency span configuration options). In case of manual mode, the behavior of the frequency observation window depends of the start (f_{start}) / stop (f_{stop}) frequency inserted. That means the final resolution (r_f) will be as expressed in (8), where (N) is the number of samples.

$$r_f = \frac{f_{stop} - f_{start}}{N} \tag{8}$$

Table I - Automatic frequency range mode dependency in function of the time window and number of samples.

Time window	Frequency range				
	Number of samples	200	400	800	1600
	f_{start}	f_{stop}	f_{stop}	f_{stop}	f_{stop}
1024 *s*	0.977 mHz	195 mHz	390.6 mHz	781.25 mHz	1.5625 Hz
512 *s*	1.95 mHz	390.6 mHz	781.25 mHz	1.5625 Hz	3.125 Hz
256 *s*	3.906 mHz	781.25 mHz	1.5625 Hz	3.125 Hz	6.25 Hz
128 *s*	7.8125 mHz	1.5625 Hz	3.125 Hz	6.25 Hz	12.5 Hz
64 *s*	15.625 mHz	3.125 Hz	6.25 Hz	12.5 Hz	25 Hz
32 *s*	31.25 mHz	6.25 Hz	12.5 Hz	25 Hz	50 Hz
16 *s*	62.5 mHz	12.5 Hz	25 Hz	50 Hz	100 Hz
8 *s*	125 mHz	25 Hz	50 Hz	100 Hz	200 Hz
4 *s*	250 mHz	50 Hz	100 Hz	200 Hz	400 Hz
2 *s*	500 mHz	100 Hz	200 Hz	400 Hz	800 Hz
1 *s*	1 Hz	200 Hz	400 Hz	800 Hz	1.6 kHz
500 *ms*	2 Hz	400 Hz	800 Hz	1.6 kHz	3.2 kHz
250 *ms*	4 Hz	800 Hz	1.6 kHz	3.2 kHz	6.4 kHz
125 *ms*	8 Hz	1.6 kHz	3.2 kHz	6.4 kHz	12.8 kHz
62.5 *ms*	16 Hz	3.2 kHz	6.4 kHz	12.8 kHz	25.6 kHz
31.25 *ms*	32 Hz	6.4 kHz	12.8 kHz	25.6 kHz	51.2 kHz
15.625 *ms*	64 Hz	12.8 kHz	25.6 kHz	51.2 kHz	102.4 kHz
7.8125 *ms*	128 Hz	25.6 kHz	51.2 kHz	102.4 kHz	
3.90625 *ms*	256 Hz	51.2 kHz	102.4 kHz		

As a user option, the instrument can be configured with four plots at the same time. The program developed can be configured with only two plots at the same time, in frequency or time domain. However and as a consequence the download of the data from instrument via GPIB-USB can be longer when high resolution line is selected and/or two plots are activated at the same time (typically for 1600 samples per frequency window takes about $250\ ms$ to download). This means user should be care about the amount of data to measure versus the time to acquire. Table II shows relation between the number of samples selected versus the number of data to extract.

During frequency measurements, this software allows plotting the signal with different spectrum units as described in Table III.

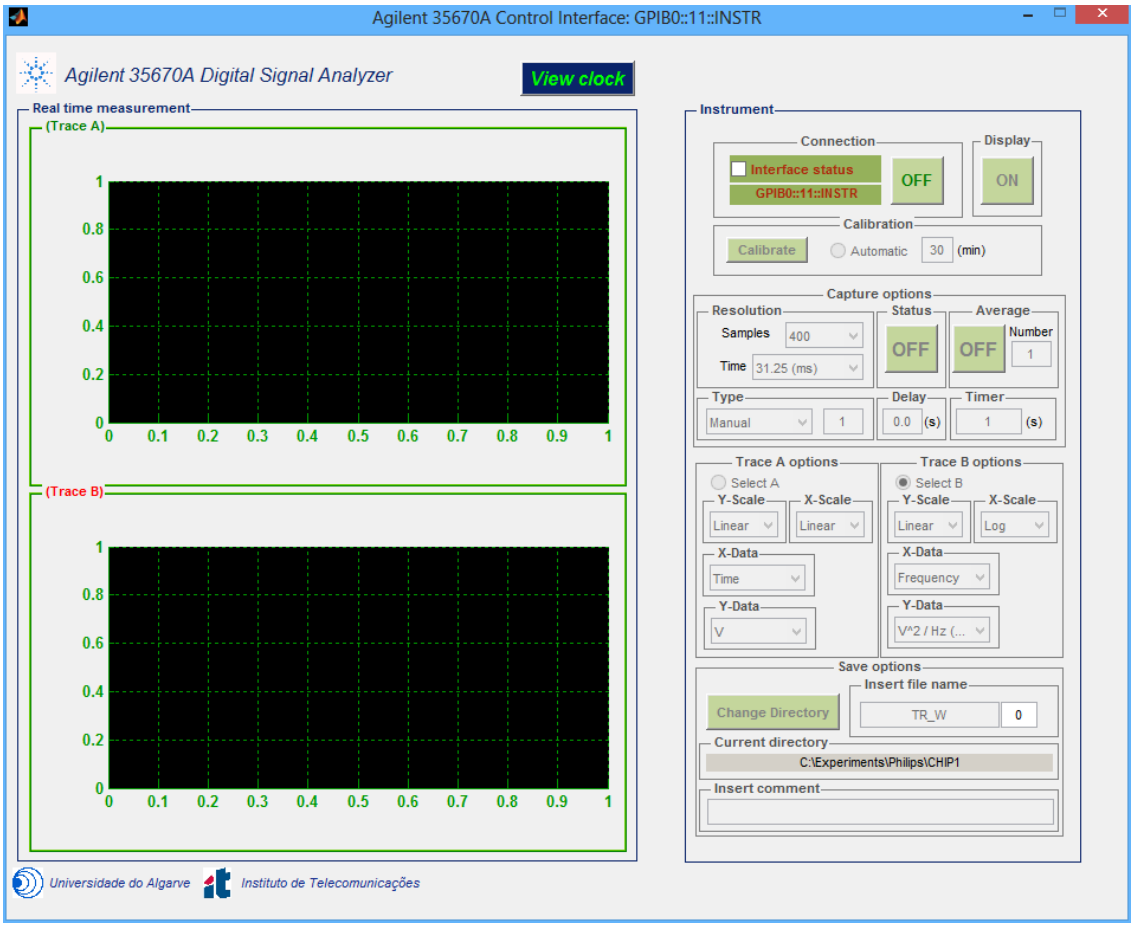

Fig. 17 – Final version of *Agilent 35670A Dynamic Signal Analyser* acquisition program.

Table II – Number of real data samples to download in function of number of samples selected.

Number of samples	Baseband	
	Frequency domain data samples	Time domain data samples
100	101	256
200	201	512
400	401	1024
800	801	2048
1600	1601	4096

Table III – Options for plotting frequency spectrum with different units.

Spectrum Units
Voltage (V)
Voltage square (V^2)
Square Root Power Spectral Density $(V/\sqrt{Hz})$
Power Spectral Density (V^2/Hz)
Energy Spectral Density $(V^2.s/Hz)$

4.3 PROCEDURES TO CARRY OUT LOW-LEVEL AND LOW NOISE SIGNALS

4.3.1 PRE-AMPLIFICATION OF THE SIGNALS (CURRENT *vs.* VOLTAGE

Signals can be amplified as voltage or current. The selection is made on the basis of the sample resistance.

A very important precaution is the overall noise figure (NF), which is the measuring unit widely used to noise performance quantification. The noise factor (F) can be defined as in Eq. (9) [61].

$$\boldsymbol{F} = \frac{\boldsymbol{SNR_{in}}}{\boldsymbol{SNR_{out}}} = \frac{\boldsymbol{1}}{\boldsymbol{G_p}} \frac{\boldsymbol{P_{n_{out}}}}{\boldsymbol{P_{n_{in}}}} \tag{9}$$

SNR_{in} and SNR_{out} is the signal-to-noise ratio at the input and the output of the amplifier, respectively. G_p represents the power gain of the amplifier, while $P_{n_{in}}$ and $P_{n_{out}}$ are the noise power at the input and output of the amplifier. In terms of mathematics, the NF is given by the noise factor expressed in dB, as in (10) [61].

$$\boldsymbol{NF} = \boldsymbol{10 \log_{10}} \left(\frac{\boldsymbol{SNR_{in}}}{\boldsymbol{SNR_{out}}} \right) \tag{10}$$

For a chain of amplifiers (as the case of multiple instruments connected in series) the overall noise factor is expressed in Eq. (11) [61].

$$\boldsymbol{F} = \boldsymbol{F_1} + \sum_{\boldsymbol{k=2}}^{\boldsymbol{N}} \left(\frac{\boldsymbol{F_k - 1}}{\prod_{\boldsymbol{n=1}}^{\boldsymbol{k-1}} \left(\boldsymbol{G_{p_n}} \right)} \right) \tag{11}$$

F_1 is the noise factor provided from the first stage of amplification, and from then can be generalised for a chain of N amplifiers, each one with noise factor of F_k and a power gain of G_{p_k} [61].

From equation (11) can be concluded that the noise performance of the amplifier is dominated by the noise performance of the first amplifier stage as long as the gain of this first stage, G_{p_1}, is large [61]. Also, due to the noise phenomena are related to the

current flowing through the sensing device, it also means that noise is generated by a random noise current source, which also depends from the resistance [25]. That is why the signal amplification decision is so important, because signals in baseband are predominantly dependent from thermal noise, which implies a pre-amplification stage implemented by low noise amplifier in order to reduce noise amplification. Having considering this, the most natural choice for amplifying the device output is to use a low noise current amplifier, even more for high resistance samples. The low noise current amplifier converts the output current noise into voltage, avoiding current to voltage conversions in the circuit which depend on other circuit parameters and therefore introduce errors [25].

The solution adopted to implement the first pre-amplification stage was to connect the experimental sensing device to a *Stanford Research* 570 (SR570), which is a commercial low-noise current pre-amplifier that operates with a battery to minimize the 50Hz power-line noise. The SR570 when is operating in low noise mode, allocates most of the gain in the front end of the instrument to decrease the magnitude of thermal noise (Johnson noise) at the output.

The final resolution of our measuring system is controlled by the resistance of the set formed by cells plus medium. For a typical value we usually have at low frequency resistance of 140 MΩ which gives a thermal noise of 2.318 $\mu V^2/Hz$. This determines our detection limit (noise floor of our measuring system cells plus electrolyte).

4.3.2 SELECTING PRE-AMPLIFIER BANDWIDTH

As an option from the adopted instrument (SR570) to implement the pre-amplification stage, the sensitivity can be adjusted, although is an option that user should use with careful. By increasing the sensitivity, decreases the frequency bandwidth to be recorded, as a consequence of loose temporal resolution. In Fig. 18 is exemplified the relation between instrument amplification bandwidth and gain.

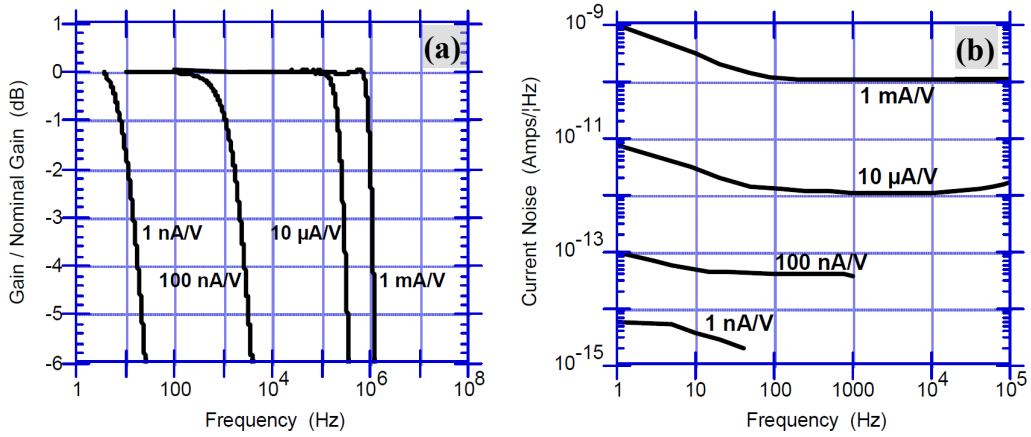

Fig. 18 – Specifications for SR570 at LOW NOISE gain mode. (a) Amplifier bandwidth and (b) current noise as function of frequency for several sensitivity settings.

Fig. 18 was retrieved from SR570 specifications manual[5]. The most important information that can be learned from Fig. 18 is the level of instrument noise floor for different sensitivity level, which means when instrument is set in LOW NOISE gain mode, for a given gain, the LOW NOISE mode allocates gain toward the front-end in order to quickly "lift" low-level signals.

The user can adjust the sensitivity within the range of $1\ pA/V$ to $1\ mA/V$, which is displayed in instrument front-panel as the product of a factor 1, 2 or 5 and a multiplier (x1, x10, x100) with the appropriate units.

The best way to acquire data in a broad frequency range using the SR570, is to select the LOW NOISE gain mode, turn all the filters OFF (select NONE at instrument front-panel), and disable all the DC bias sources. Considering both current and bias voltage sources at OFF state, a standard recommended procedure to acquire a frequency ranges using different sensitivities levels, is the one described on table IV.

[5] http://www.thinksrs.com/products/SR570.htm, available at 17/09/2013.

Table IV – Standard recommended procedure to acquire a frequency ranges using different sensitivities levels (It is recommended to use at least 10 averages per each frequency window).

Sensitivity	Gain mode: LOW NOISE			
	Frequency		Temporal	
	Window	Resolution	Window	Resolution
1 µA/V	0 Hz - 200 Hz	125 mHz	8 s	2 ms
1 µA/V	200 Hz - 1 kHz	125 mHz	2 s	488 µs
1 µA/V	1 kHz - 13.8 kHz	375 mHz	125 ms	30.5 µs
10 µA/V	13.8 kHz - 26.6 kHz	7.5 Hz	125 ms	30.5 µs
10 µA/V	26.6 kHz - 52.2 kHz	16 Hz	62.5 ms	15.25 µs
100 µA/V	52.2 kHz - 103.4 kHz	32 Hz	31.25 ms	7.63 µs

All values for resolution calculation where taken in account that *Agilent 35670A* is selected for maximum temporal resolution; this means the number of samples considered are *1600* (which implies the measuring of *4096* samples in time domain, see Table II).

Another aspect to take into account is averaging. The use of averaging is not desirable when single events may occur.

4.3.3 CONVERSION OF NOISE SPECTRAL DENSITY TO NOISE CURRENT SPECTRAL DENSITY

Due to the dynamic signal analyzer measures the noise spectral density in voltage units, mathematical calculations are needed in order to obtain the desired results of current noise spectral density. This is done using the following transformation.

$$\boldsymbol{S_I(f) = (N_{meas} \cdot S_{SR570})^2} \tag{12}$$

where N_{meas} represents the noise measured by the analyzer expressed in $V/\sqrt{Hz}$ and S_{SR570} is the sensitivity of the amplifier [25].

4.4 CELLS CULTURE AND PROTOCOL

Two types of commercial available immortal cells cultures were used in this study: **(i)** C6 glial cells from *Rattus norvegicus*, rat, and **(ii)** Neuro-2A neuroblast cells from *Mus muscullus*, mouse. Optical photographs of the two types of cells are shown in (Fig. 19) and (Fig. 20) respectively.

4.4.1 CRITERIA FOR CELL SELECTION

Rat glioma C6 cells are glial cells from brain tissue, they are adherent cells [38], and their morphology is fibroblast. C6 glial cells are frequently used to study cellular functions and cell signalling. These cells have sodium channels, calcium channels and potassium channels [52]; furthermore they have receptors to neurotransmitters such as ionotropic glutamate receptors (GluRs) and ionotropic GABA receptors ($GABA_a$ and $GABA_c$) as well as glycine receptors [53][54].Glial cells are not electrically excitable, however, they can generate intracellular Ca^{2+} waves travelling from one glial cell to the next [51]. Calcium signalling might thus be a form of glial excitability enabling these cells to integrate extracellular signals, communicate with each other and exchange information with neurons.

In excitable cells, the initiation of the cytoplasmic Ca^{2+} signal results from both Ca^{2+} entry via plasmalemmal voltage or ligand-gated Ca^{2+} channels and Ca^{2+} release from internal pools, while in non-excitable cells it is the release of Ca^{2+} from intracellular pools that dominates.

Both mechanisms results in an increase in the intracellular Ca^{2+} concentration ($[Ca^{2+}]_i$) , due to a steep Ca^{2+} gradient between the extracellular fluid or intracellular compartments. Activation of Ca^{2+} entry via voltage-gated channels needs cell depolarization [55].

Previous work had shown that hypotonic media-induced swelling of astrocytes caused membrane potential depolarisations sufficient to open such channels. The removal of extracellular calcium also abolished swelling-induced K^+ and Cl^- efflux. Extracellular Ca^{2+} then enters the cell, leading to a sustained increase in intracellular free calcium ($[Ca^{2+}]_i$), triggering activation of Ca^{2+}- dependent ion channels and the release of K^+ and Cl^- [57].

Mouse Neuro-2A cells are neuroblast cells from brain tissue and are adherent cells [38], their morphology are neuronal and amoeboid stem cells. Neuro-2a cells are neurons capable to produce action potentials, and have (among others) sodium, calcium and potassium channels [58].

They generate electrical signals to convey information over substantial distances and to transmit it to other cells by synaptic connections means. These signals ultimately depend on changes in resting electrical potential across the neuronal membrane. A

resting potential occurs because nerve cell membranes are permeable to one or more ion species subject to an electro - chemical gradient. More specifically, a negative membrane potential at rest results from a net efflux of K^+ across neuronal membranes that are predominantly permeable to K^+.

In contrast, an action potential occurs when a transient rise in Na^+ permeability allows a net flow of Na^+ in the opposite direction across the membrane that is now predominantly permeable to Na^+. The brief rise in membrane Na^+ permeability is followed by a secondary, transient rise in membrane K^+ permeability that repolarizes the neuronal membrane and produces a brief undershoot of the action potential. As a result of these processes, the membrane is depolarized in an all-or-none fashion during an action potential. When this active permeability changes subside, the membrane potential returns to its resting level because of the high resting membrane permeability to K^+ [58].

4.4.2 CELL GROWTH ON SENSING DEVICE

C6 glial cells were cultured in F-12K Nutrient Mixture, 15% of Horse Serum, 2,5% of FBS and 1% of penicillin and streptomycin. Besides that, cells were maintained in a humidified atmosphere at 5% of CO_2 and 37ºC. The medium was changed every two days [38].

When cultures were confluent, the devices were in a UV camera during 15 minutes and after that, they were treated with poly-lysine provided from Sigma-Aldrich, and cells were placed on the electrodes. Cultures were used when they were confluent. We applied 60µL cell suspension of C6 cells on the devise and incubate them at 37ºC and 5% CO_2. At the last experiments the devices had approximately $4{,}756*10^5$/well.

After starting the measurements was added 2-10 mM of $CaCl_2$, and then were added 2 µM of TTX which will cause a voltage and frequency-dependent inhibition of the rapid inward sodium current [55][56].

Neuro-2A cells were cultured in DMEM (1x), 10% fetal bovine serum (FBS) and 1% of penicillin and streptomycin. The cells were maintained in a humidified atmosphere at 5% of CO_2 and 37ºC. The medium was changed every two days [38].

When the cultures were confluent, the devices were in a UV camera during 15 minutes and after that, they were treated with poly-lysine provided from Sigma-Aldrich

and cells were placed on the electrodes. Cultures were used when they were confluent. We applied 60µL cell suspension of Neuro-2a cells on the device and incubate them at 37ºC and 5% CO_2.

After starting the measurements were add 30mM of KCl, and then was added 2µM of TTX that cause a voltage and frequency-dependent inhibition of the rapid inward sodium current [59][60].

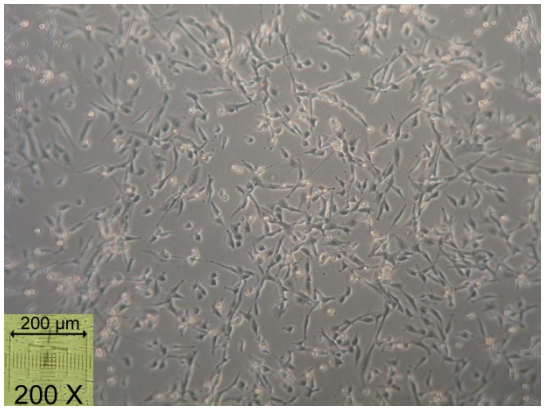

Fig. 19 – Optical photograph of C6 glial cells in culture.

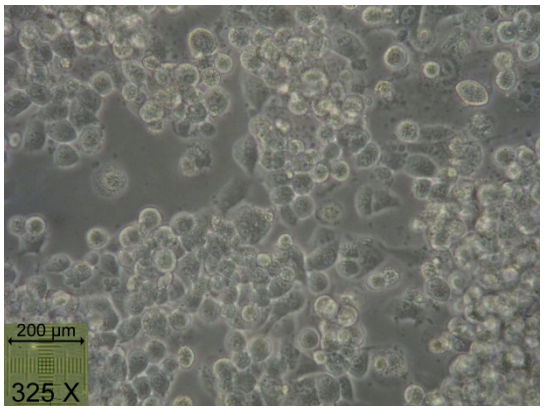

Fig. 20 – Optical photograph of neurons (Neuro-2A) in culture.

Chapter 5

RESULTS

This chapter presents the main results obtained using sensing devices to measure extracellular bioelectrical activity *in vitro*.

5.2 EQUIVALENT MODEL FOR EXTRACELLULAR DEVICE INTERFACE WITH CELLS IN VITRO

Electronic devices based on metal-insulator semiconductor field effect transistors (MISFET) type devices without a semiconductor channel (see Fig. 15) were used as sensing devices. The metal electrodes are gold tracks.

A particular characteristic of metals and semiconductors when immersed in liquids is the existence of a double-layer (DL) capacitance (C_{DL}) also known as Stern layer. When a metal is placed into ionic liquid, an equilibrium condition is established once the charge transfer between the metal and the solution is equal. The electric field on the interface generated by electron transfer causes the formation of an inner Helmholtz plane (IHP) and an outer Helmholtz plane (OHP). The net reaction induces the creation of an electric double layer, which is also an electrified interface describing the interphase region at the electrolyte boundary [62].

When cells are released in electrolyte medium, they start to spread on the microelectrodes, and cells adhere to the substrate. But there is still a minute volume of electrolyte between the cells and the microelectrodes; thus, a solid-liquid interface on the electrode surfaces is formed. The electrochemical properties of the interface are the basis of the sensing mechanism of MEA [62].

It is possible to generalize an equivalent circuit of metal-electrolyte interface, using the Randles model, as shown in Fig. 21. In the circuit, an interfacial capacitance (C_I) is in parallel with charge transfer resistance (R_t) and diffusion related Warburg element (R_W and C_W). The spreading resistance (R_S) represents the effect of current spreading from the localized electrode to a distant counter electrode [62].

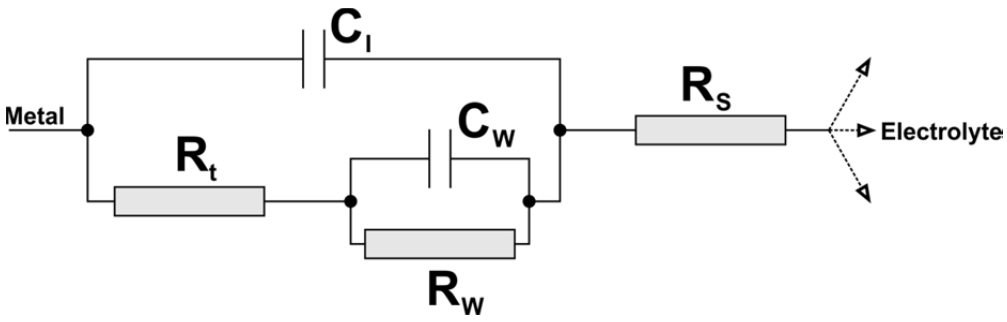

Fig. 21 – The equivalent circuit of metal-electrolyte interface [62].

Because of the electronic device in test allows the conduction of electrical signals at the substrate, a new approach where made in order to find if extracellular stimulation is possible to reach by application of electronic pulses at the substrate, that from now on will be called the gate. In Fig. 22, can be perceived that device structure is similar to a FET transistor, but without channel between source and drain. Thus, takes origin a new equivalent and more complex circuit as predicted by using Randles model in Fig. 21.

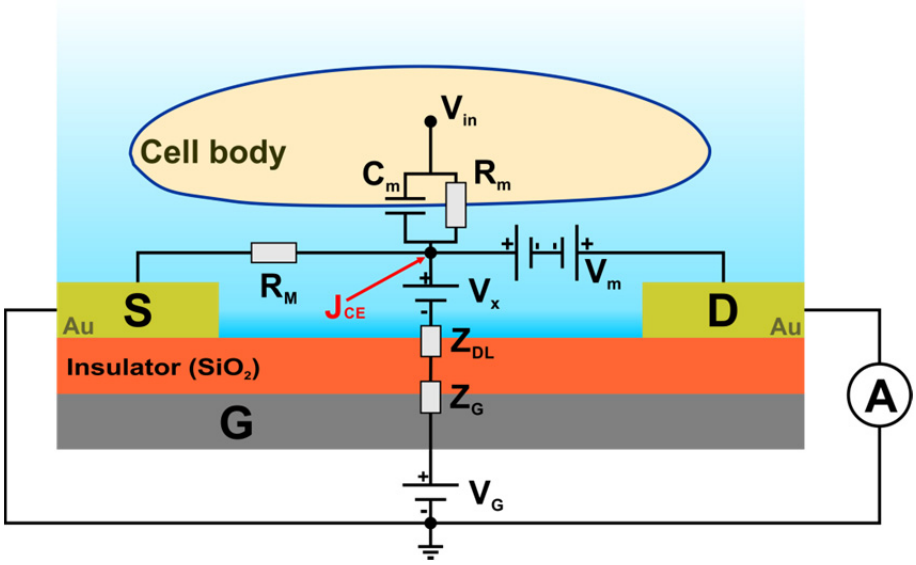

Fig. 22 – The equivalent circuit model of signal pathway in the system. V_{in}: the intracellular potential; C_m and R_m: the capacity and resistance of cellular membrane; J_{CE}: the junction between the cell and electrode; R_M: the sealing resistance between the cell and device surface; V_x: the potential difference imposed by V_G; V_m: the extracellular potential difference resulted from V_x and V_{in}.

The new equivalent circuit (Fig. 22) of the signaling pathway illustrates how a biological signal (biochemical) is converted into an electrical one. In synthesis, there are three main components in the equivalent circuit. Firstly, the trans-membrane potential functions as an electric source (V_{in}). Secondly, the parallel circuit of C_m and R_m expresses an overall effect of the cellular double-lipid layer structure, ion channels and cellular signal pathway. Finally, the electrolyte between the cells and electrodes induces part of the current to leak out to the bulk medium (source is connected to ground). This

effect, is expressed as the resistance from the medium R_M. The current flowing through the membrane is the sum of the ionic current (I_{ionic}) that flows from in-to-out, and from out-to-in as represented in Fig. 8. Due to the R_M, the recorded signal at the point J_{CE} can reflect the trans-membrane potential, however, as R_M tends to infinity, the voltage at the same node would correspond to the intracellular potential.

Therefore it is important to know how the potential of the DL changes with time, and also upon the application of a voltage step or a train of voltage pulses. In Fig. 23 can be observed the experimental setup of the sensing device, where the voltmeter used was the *Keithley 2182A* and the voltage source was the *Agilent 33220A*.

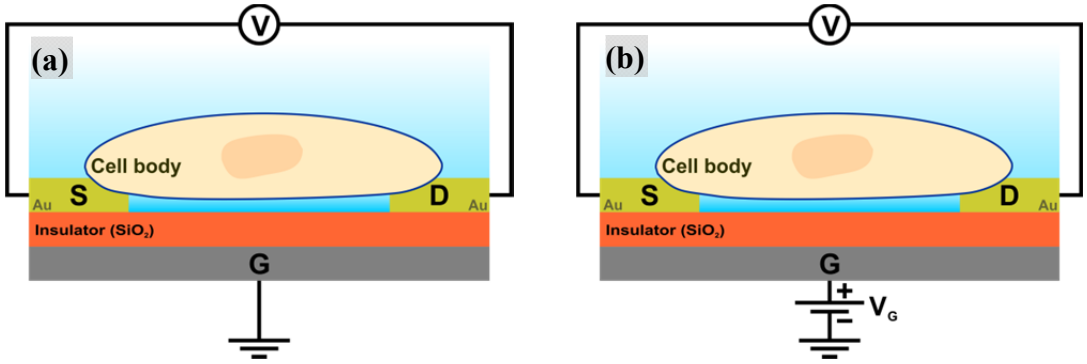

Fig. 23 – Schematic diagram of the sensing device to perform DL potential differences measures.

Fig. 24 (a) shows how the potential of the DL changes with time, when substrate (gate) is grounded, as proposed in Fig. 23 (a). First experiment was made without cells presence, and second with C6 glial cells in top of device surface. In Fig. 24 (b), was performed an experiment as proposed in Fig. 23 (b). C6 cells were adherent in top of the sensing device before the application of a programmable periodic pulse train of 20 s periods, amplitude of 4 V and 50% duty cycle, during 240 s, at the gate.

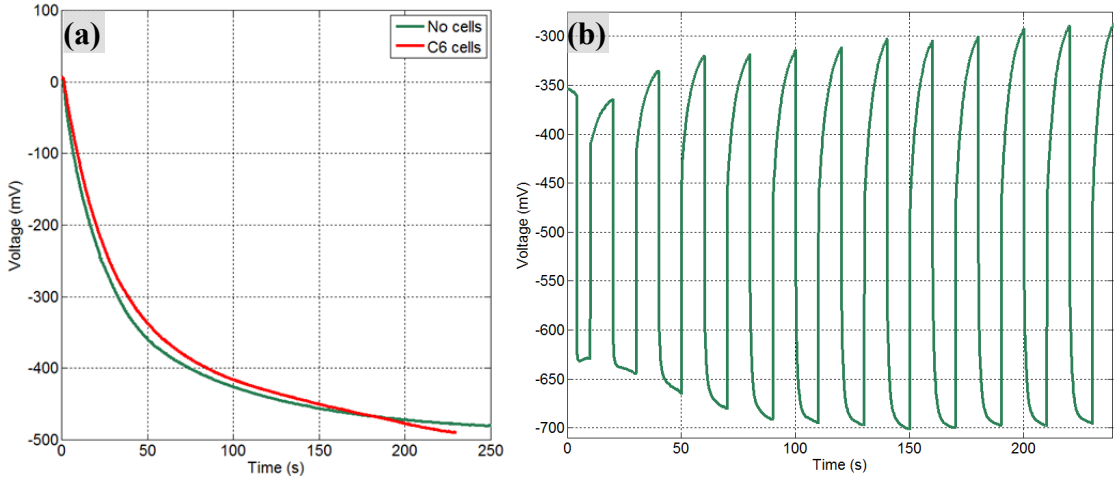

Fig. 24 – The DL effect in a MEA device. (a) Difference of potential in sensing device with and without cells presence. (b) Application of periodic pulse train in presence of C6 glial cells.

In Fig. 24 (a), is verified that isn't the presence of cells but from ionic liquids (electrolyte medium) that triggers a DC voltage at the electrodes (about $500\,mV$), due to the DL effect as explained before. That voltage, is represent in Fig. 22 as the V_x. Finally, Fig. 24 (b) presents the effect of electrode polarization with positive and negative charges, given the direction of equilibrium condition. Due to short pulse period the difference between peaks remains at about $400\,mV$, which means high frequencies processes reach equilibrium state very fast, remaining the low frequencies processes, that as is noticed in Fig. 24 (a), in an infinite time the voltage tends to $500\,mV$ to reach a new equilibrium state.

5.3 ELECTRICAL MEASUREMENT

Different approaches will be made in order to perform electrical measuring experiments, as impedance analysis, thermal noise, spectral analysis, and time domain analysis after electric and chemical stimulus.

5.3.1 SMALL-SIGNAL IMPEDANCE TECHNIQUES

By culturing cells over one or more electrode contacts, changes in the effective electrode impedance permits a noninvasive essay of cultured cell adhesion [39], spreading [41], and mobility. Impedance measurements rely on the observation that living cells are electrical insulators at low signal frequencies. As cells grows or migrate to increase coverage over an electrode surface, the effective electrode impedance rises.

Impedance measurements have found practical use in the rapid analysis of meat quality, the detection of food pathogenic bacteria [42], cell-substratum spacing and cell death [40]. In a recent report it was even shown, that a glucose-sensing device with a rather linear response could be realized based on an impedance sensor structure grown with fibroblasts [42]. Metabolic products created during the growth of microorganisms can also be detected by impedance changes because they modify the composition of the medium, changing the ionic content, which, in turn, resulted in conductivity changes of the culture broth.

There are ongoing studies directed to the monitoring of bacteria growth [45], motility, spreading and mortality of insect cells [46] drug screening using cells associated with electrode surfaces.

The impedance magnitude as well as the frequency dependence will depend on the activity of the cells and their adhesion to the microelectrodes.

In order to understand the changes in the small-signal impedance caused by attached cells in the device, it is convenient to model the system by a two RC network represented in Fig. 25. Basically, one of the RC networks takes into account the surface where the cells are attached and the other RC network the electrolyte medium. Since the capacitance of the electrode area (double-layer capacitance) is higher than the electrolyte solution capacitance, the system exhibits a Maxwell-Wagner relaxation at a particular frequency. A typical behavior of the frequency dependence of the capacitance (C) and conductance (G) represented as loss $\left(loss = 1/(R\omega)\right)$ where R is the resistance and $\omega = 2\pi f$ the angular frequency.

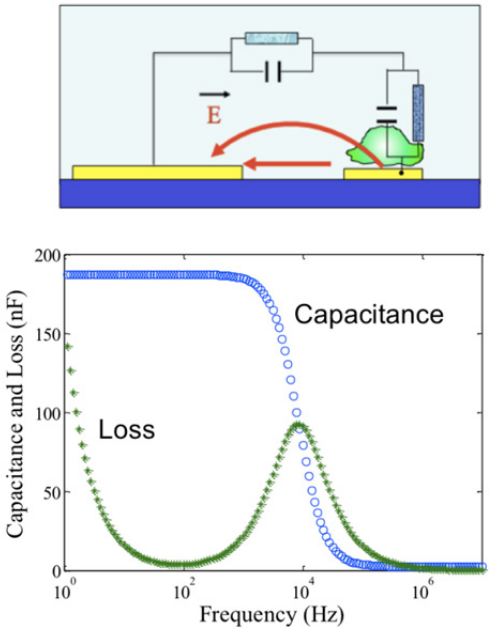

Fig. 25 – Top figure shows a schematic diagram a cell on a solid surface and the corresponding equivalent circuit that takes into account the cell and the electrolyte medium. Bottom figure shows the ideal frequency dependence of the capacitance and loss of system.

As cell deposition and adhesion progress, the following changes occur in the impedance:

- Increase slightly in the low frequency capacitance.
- The relaxation peak moves to lower frequencies (increasing coating of the surface).

Examples of the above behavior are show in the following figures. Fig. 26 shows the changes in the frequency dependence capacitance and conductance as the cells suspended in solution start to attach to the electrode surface. When a fast train of electrical pulses ($5\,V$, $200\,\mu s$ long) is applied to the surface causes a partial cell

detachment and a rapid movement of the relaxation frequency to a higher frequency. This effect is shown in Fig. 27 and in Fig. 28.

The addition of chemical species often release ions, which also cause small movements in the relaxation frequency. This analysis is more complex because the movements depend on how the ionic species interact with the ones already present in the system and how they affect the cells. In general an increase in the electrolyte conductivity moves the loss relaxation peak to higher frequencies. A high ionic conductivity may give rise to a low frequency tail in the loss as show in Fig. 29.

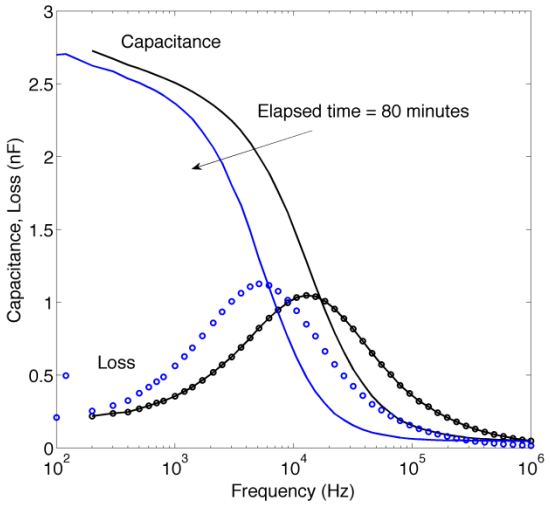

Fig. 26 – Changes in the capacitance and loss as the cells sediment and attach to the sensing surface.

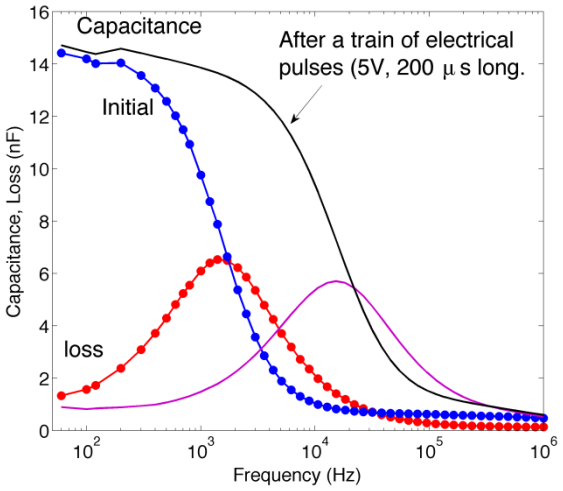

Fig. 27 – Changes induced in the cell/electrode impedance after a train of electrical pulses.

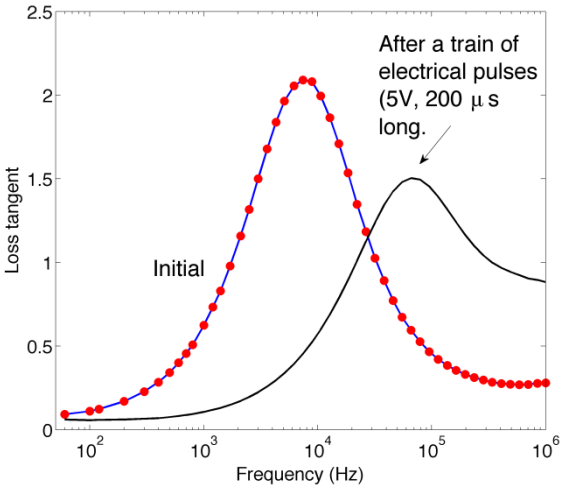

Fig. 28 – Changes induced in the cell/electrode impedance represented as a loss tangent

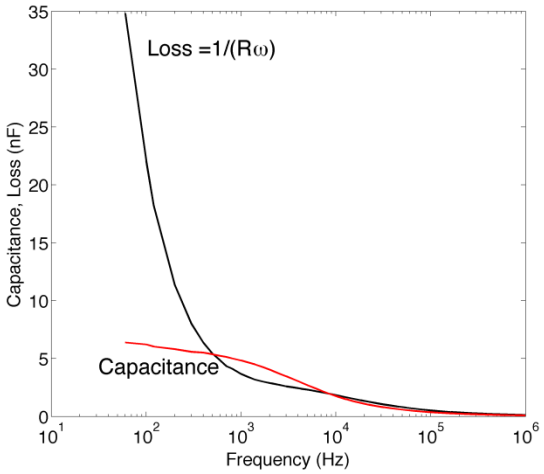

Fig. 29 – The behavior of the loss and the capacitance when the system has a high DC conductance caused by the electrolyte medium.

5.3.2 BIOELECTRONIC ACTIVITY UPON ELECTRICAL STIMULATION

A different approach of the common micropipette electric pulses to induce intracellular action potentials is to characterize the cell-electrode junctions. That can be achieved by probe the spontaneous fluctuations of the extracellular voltage or current, when different electric stimulus is applied in the device gate (as suggested in Fig. 30).

After several experiments, it was determined that electrical stimulus using AC coupled voltage pulses, should obey to some rules associated to the typical noise current behavior. In Fig. 31, can be visualized some of the pulses train behavior, where was applied in (a): periodic pulse train of 40 s period amplitude of 1 V and 25% duty cycle; in (b): periodic pulse train of 100 s period amplitude of 1 V and 50% duty cycle; in (c): periodic pulse train of 100 s period amplitude of 5 V and 50% duty cycle; and in (d): periodic pulse train of 200 μs period amplitude of 6 V and 50% duty cycle. The duration of each training pulse last approximately five to ten minutes. The ammeter used was the *Keithley 487* and the voltage source was the *Agilent 33220A*.

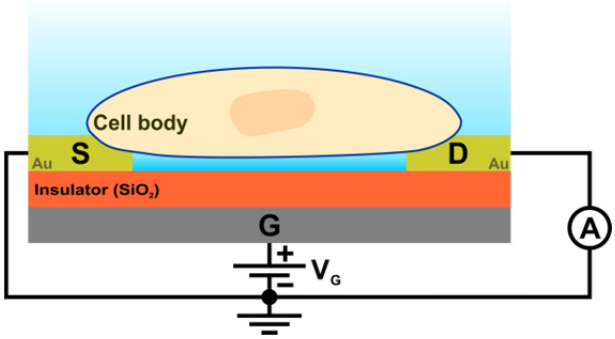

Fig. 30 – Experimental set-up to pulse the sensing device with a train of AC coupled voltages pulses (across the dielectric layer).

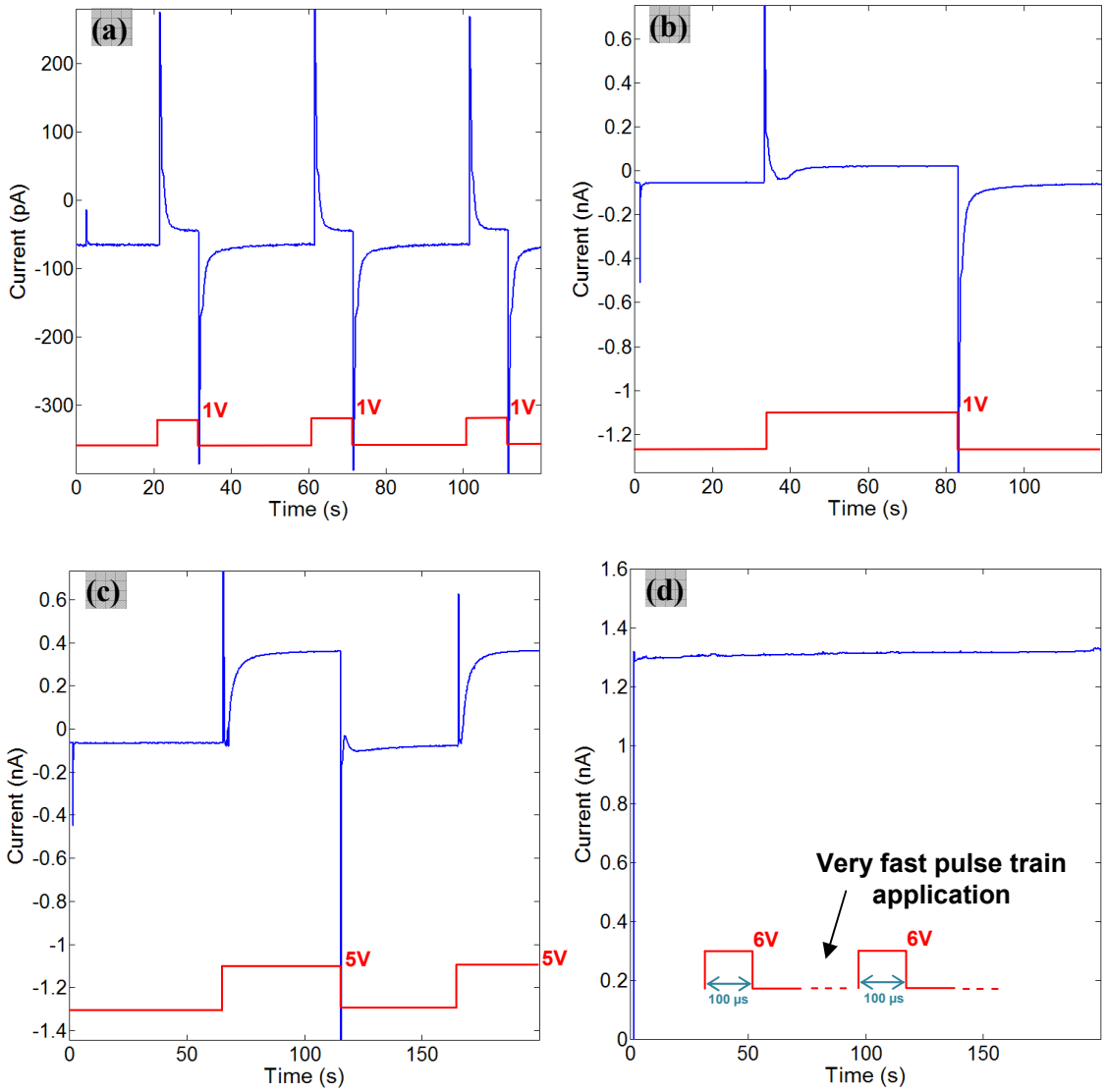

Fig. 31 – Electric current behaviour produced by different electrical stimulus using AC coupled voltage pulse train, in order to train C6 cells.

At the Fig. 32, it was finding the periodic extracellular response from C6 glial cells. Due to C6 cells are not neurons, they do not generates action potentials by it self's, still the processes of polarization and depolarization of charges, appears to overload the trans-membrane channels and pumps, and forces cells membrane to exchange ions from in-to-out and out-to-in.

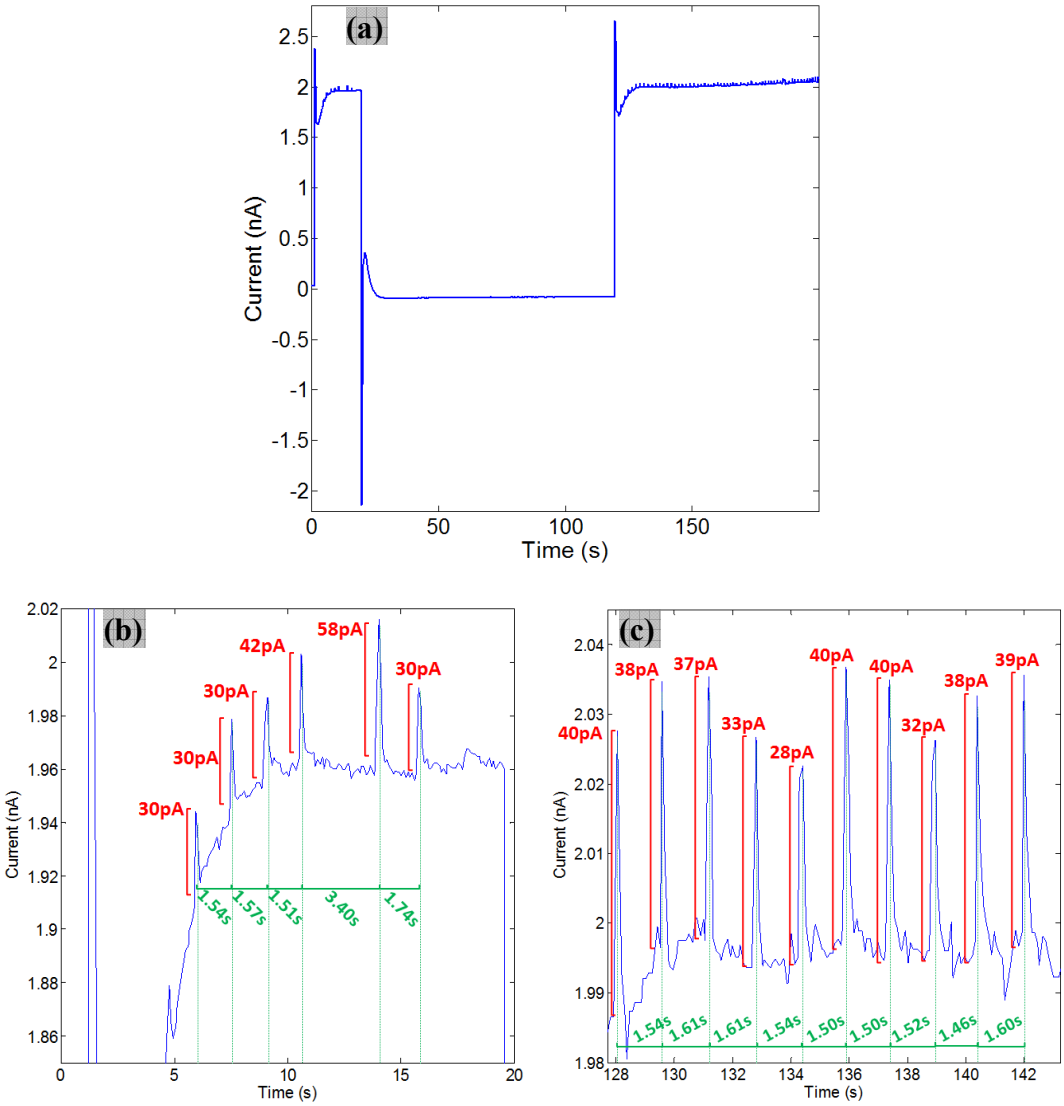

Fig. 32 – C6 glial cells extracellular currents leaks due to membrane charges overload. (a) . (b) Non-periodic response. (c) Periodic response.

The periodic responses frequency range is about $0.6\sim0.7\,Hz$, and with approximately 38 pA of current amplitude above DC current.

Another approach is to pulse the device with a train of AC coupled voltages pulses (across the insulating dielectric layer), where a dramatic change occurs in the noise. A detailed view of this type of noise is shown in Fig. 33.

The magnitude of the noise increases dramatically and a periodic current burst is observed. Fig. 34 shows a detailed view of these bursts. These signals have a frequency of $0.2\,Hz$ and can be recorded for periods as long as 30 minutes. The addition of tetrodotoxin (TTX), as shown in Fig. 35, increases further the magnitude of the noise, however the periodic nature of the burst is no longer clear observed.

The findings suggest that a cooperative phenomenon is induced in the cells after the electrical stimulus in the presence of chemical neurotransmitters exposure.

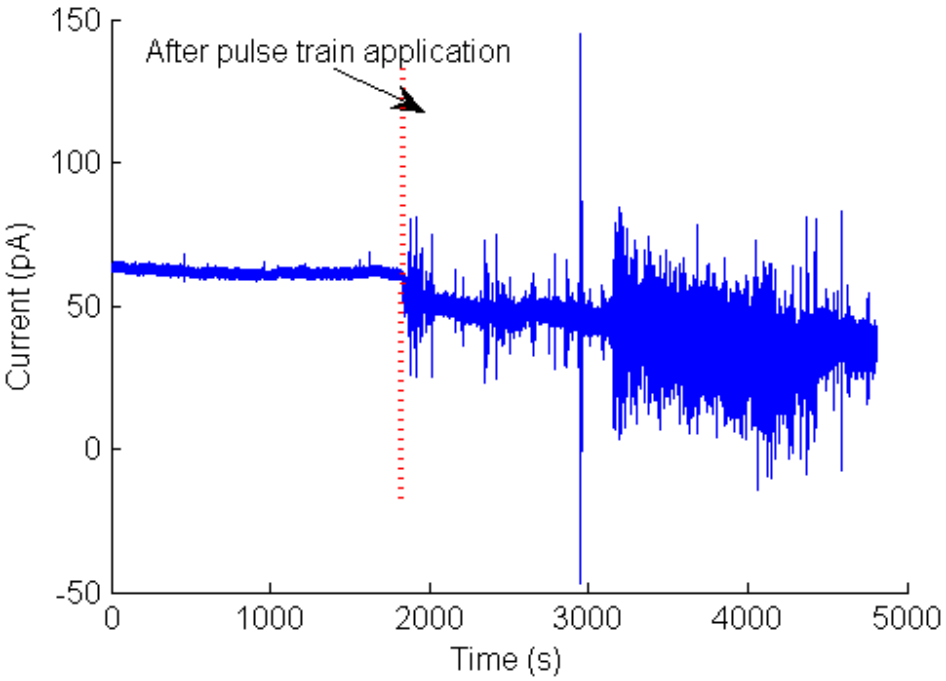

Fig. 33 – Time dependence of the electrical noise after the addition of calcium, electrical excitation.

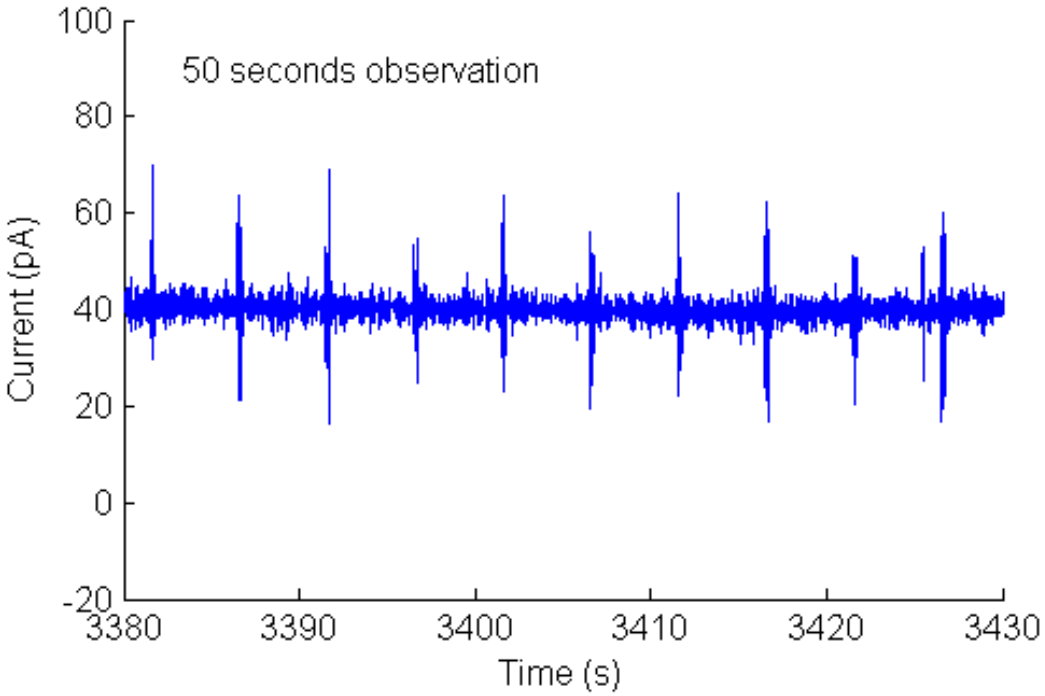

Fig. 34 – Periodic burst of noise with a frequency of 0.2 Hz were observed after calcium addition followed by an electrical stimulus.

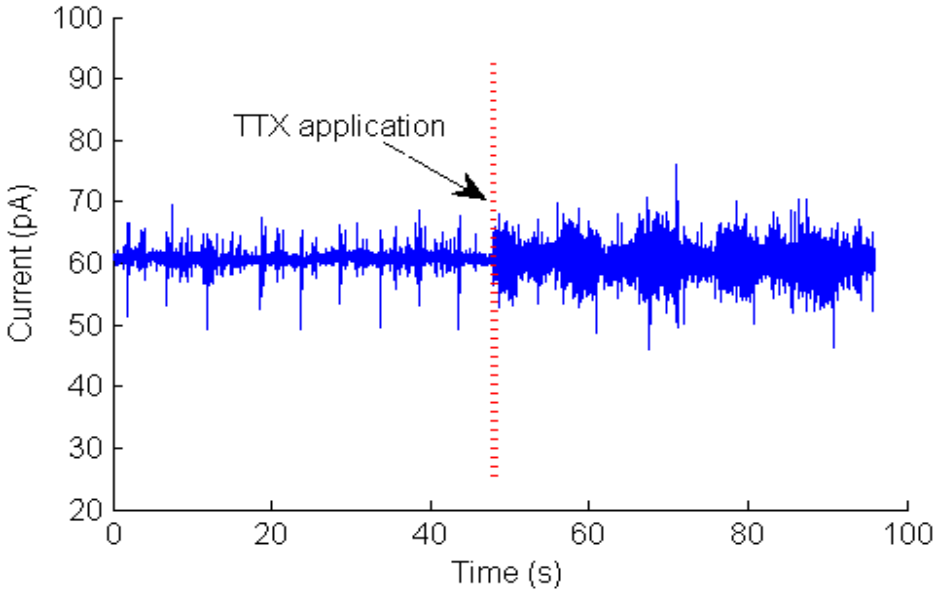

Fig. 35 – Close look at the shape of the noise after the electrical stimulation and addition of TTX.

Bioelectrical activity was also recorded in neuronal cells (Neuro2A cells described previously in 4.4.1). The cells were exposed to potassium to induce the generation of action potentials. Upon KCl (30 μM) addition dramatic changes in the cell bioelectrical activity were observed (see Fig. 36). A detailed view of the time traces revels signals similar to action potentials (see the time traces in Fig. 37).

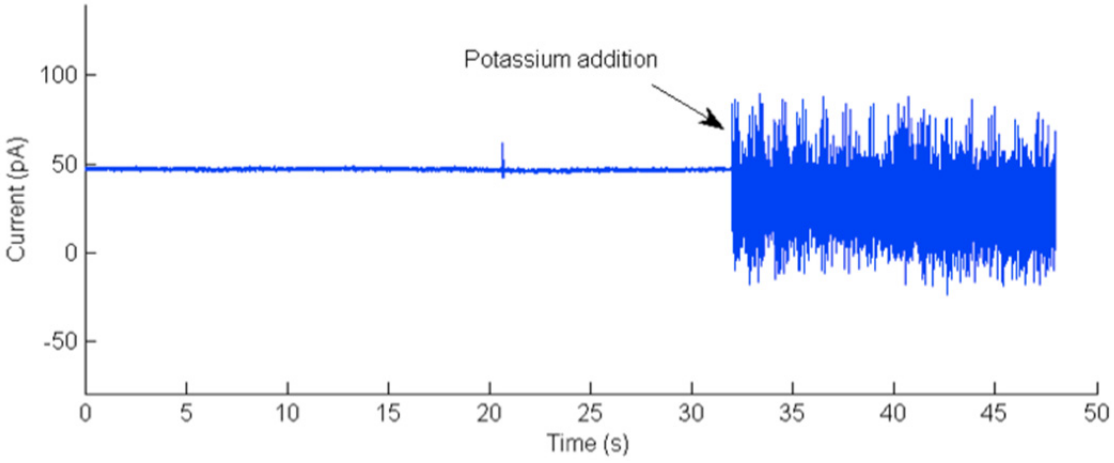

Fig. 36 – Changes in the current fluctuations measured after the addition KCL (30 μM) to Neuro2A cells.

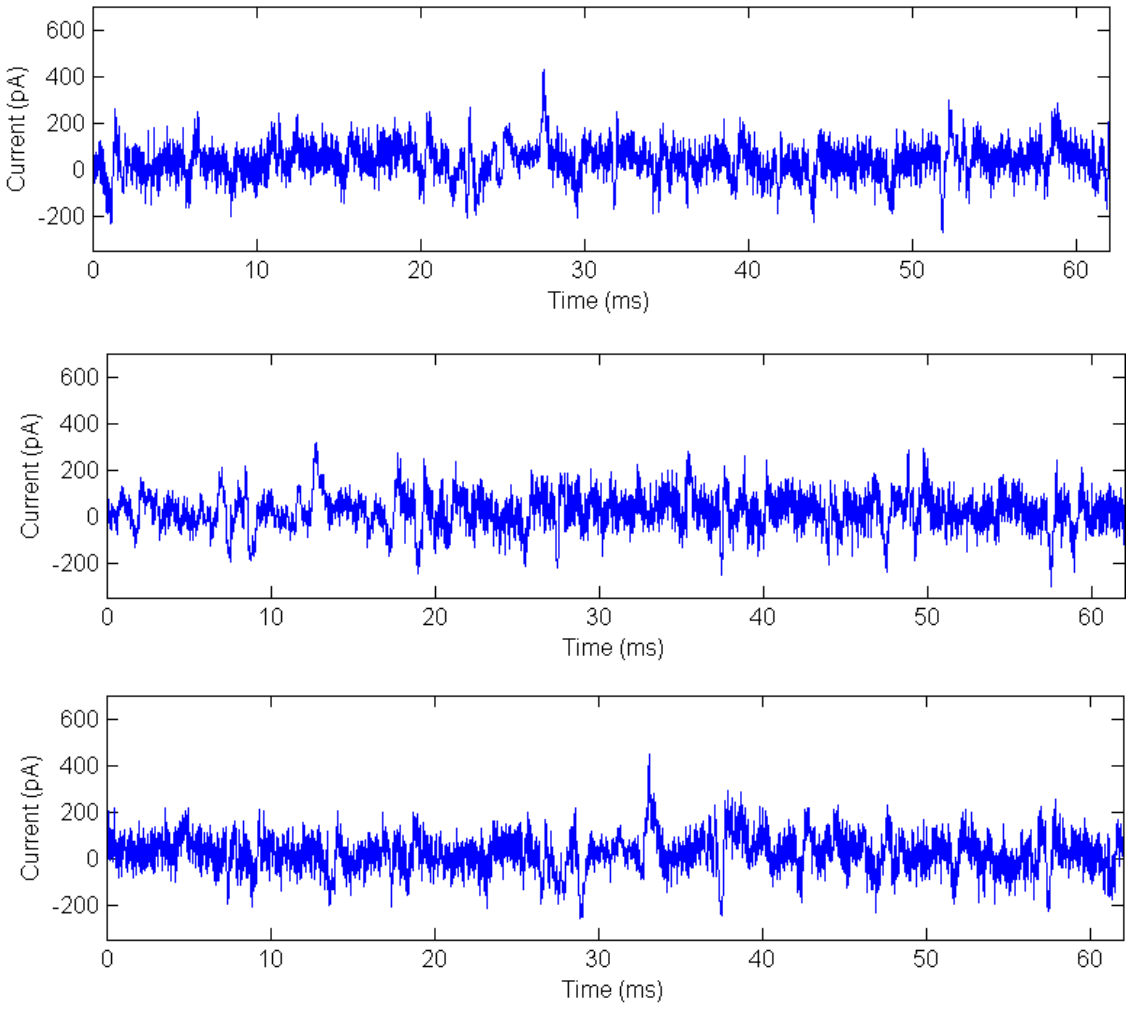

Fig. 37 – Time traces of the current fluctuations after the addition of KCl (30 µM) to Neuro2A cells.

5.3.3 SPECTRAL ANALYSIS OF THERMAL NOISE AND BIOELECTRONIC ACTIVITY UPON EXPOSURE TO CHEMICAL AGENTS AND ELECTRICAL STIMULUS

Cell-electrode junctions were probed by measuring the spontaneous fluctuations of the extracellular voltage or current. We probed current fluctuations in a spectral range from $1\,mHz$ to $102.4\,kHz$ using arrays of planar gold microelectrodes on thermal oxidized silicon wafers. The quantitative interpretation of the electrical noise provides information about cell health state and cell bioelectrical activity.

An explanation was made previously in 2.4 for noise measurements, where in summary can be considered that the two main contributions of the measured signals are:

(i) Thermal equilibrium noise.

(ii) Nonequilibrium noise or bioelectrical signals.

In Fig. 38, is represented the device set-up for thermal noise and bioelectrical signals measurements. A periodic pulse train of 600 μs period amplitude of 5 V and 32% duty cycle was applied during 60 s. The train of pulses was AC coupled to the insulating SiO_2 surface while the gold terminals were kept ground. The voltage source was the *Agilent 33220A*.

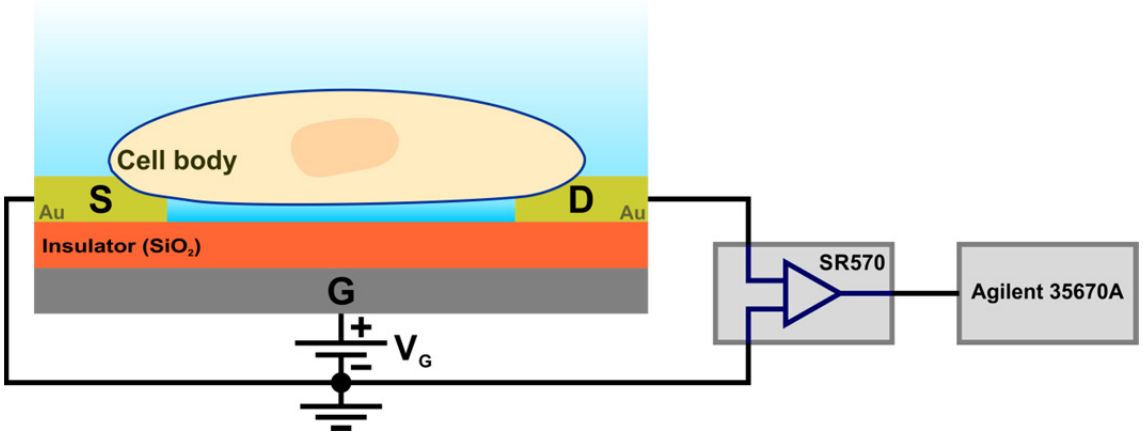

Fig. 38 – Experimental set-up to perform thermal noise and bioelectrical signals measurements.

Fig. 39 shows the power spectral density (PSD) of C6 cells deposited on 60 μL of medium in the gold MEA surface. The noise has a clear plateau between 1 and $10Hz$. The noise rises again for frequencies below 1 Hz. The high frequency region ($f > 10Hz$) follows $1/f^2$ behaviour. The addition of dopamine increases significantly the low-frequency slope ($f < 1\,Hz$). The effect is metastable and after some time (30 minutes) the original spectrum is restored as show in Fig. 40. The same behaviour can be observed by plotting the histograms of time traces as function of time. The average DC level of the histogram moves to lower current as the time elapses after neurotransmitter exposure.

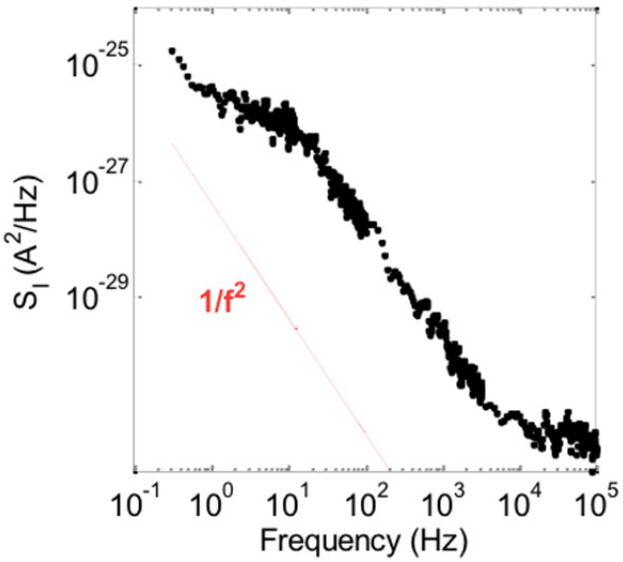

Fig. 39 – Current power spectral density of C6 cells deposited on top of gold surfaces.

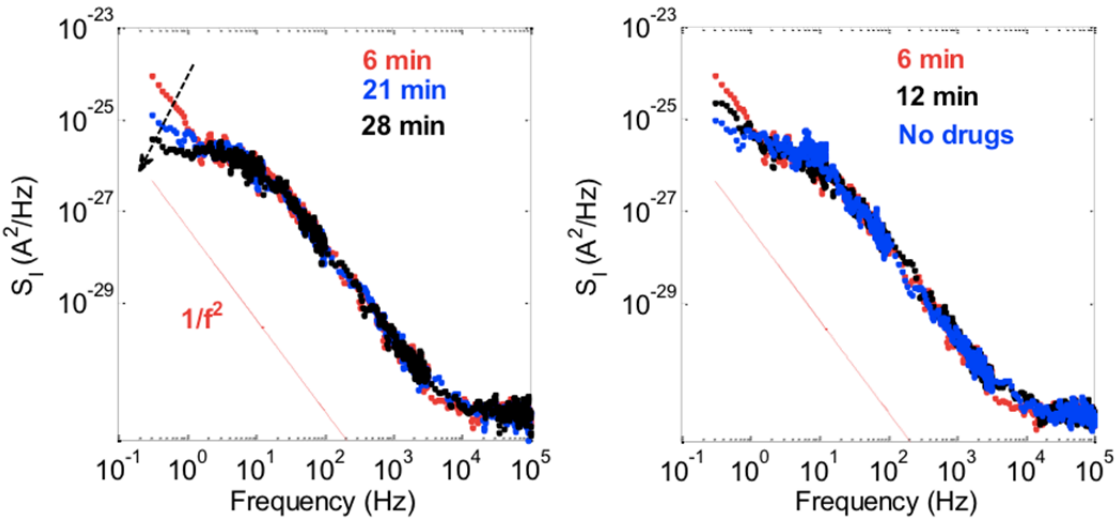

Fig. 40 – The effect of adding dopamine to C6 cells on the noise spectra.

The addiction of extracellular stimulation with neurotransmitters such as dopamine in higher concentration ($> 5\mu M$) causes a shift to lower values of the average DC level of the noise current. This is clearly seen when the time domain traces are analysed in a form of histograms. A typical result is shown in Fig. 41. All the evidences suggest that the C6 glial cells get detached from the electrode surface possible because some of them are dying as consequence of neurotransmitter substance exposure. The average noise amplitude decreases because the membrane is no longer attached to the solid surface. The average resistance contributing to thermal noise decreases as the cells get detached from the solid surface.

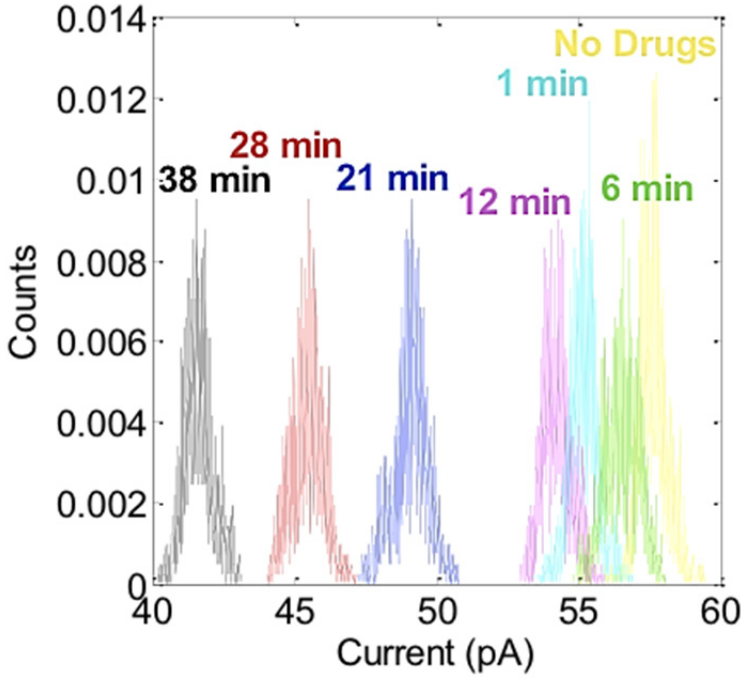

Fig. 41 – Histogram of time dependent traces after the addition of dopamine. Upon addition of extracellular stimulation the average current moves to lower values with time.

Fig. 41 shows the time dependence of the noise of C6 glial cells in culture on top of gold MEA using the thin film transistor structure shown in Fig. 38. The addition of calcium chloride solution ($2mM$ and $10mM$ in concentration) cause measurable changes in the observed noise recorded as function of time. In Fig. 42 (a) can be perceived that the current PSD with the addition of calcium ($2mM$) only suffer perturbations in frequencies range below $100\ Hz$, and after the addition of tetrodotoxin (TTX) the current PSD level is restored to the original spectrum. Fig. 42 (b) represents a zoom from the previous Fig. 42 (a) for frequencies range of $f\ < 100\ Hz$ and where can be verified that the increase level of current PSD after the addiction of calcium, means that the activity as function of time is more confluent. That same observation can be also verified in Fig. 33. From the previous Fig. 40, there was observed that high frequency region ($f\ > 10\ Hz$) follows $1/f^2$ behaviour, while in Fig. 42 (a) and (c) the same is observed but for $f\ > 1\ kHz$. The findings suggest the use of approximately $4\ mL$ instead of the $60\ \mu L$ of C6 glial cells medium (as used with dopamine experiment), represents a higher volume of ions in the total amount of solution, which are related with the R_M (electrolyte medium resistance as show in Fig. 22) that leads to a lower resistance value, and consequently the trans-membrane potential difference measured is less perceptible.

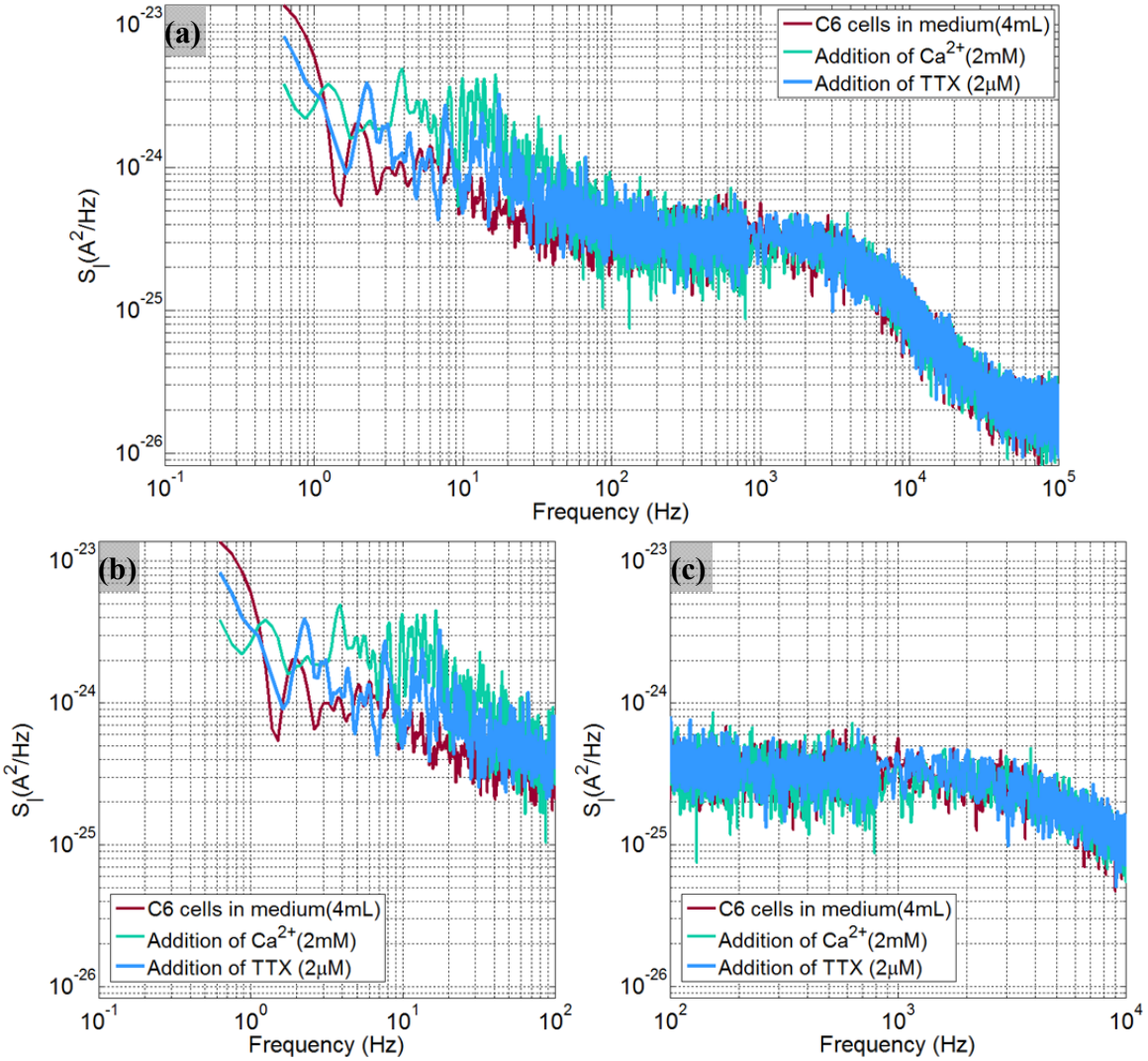

Fig. 42 – Current PSD of C6 glial cells deposited on top of gold MEA surfaces. (a) Full view of frequency range. (b) Zoom for frequencies range 0.1 to 100 Hz. (c) Zoom for frequencies range 0.1 to 1 kHz.

5.3.4 SUMMARY OF THE INFORMATION PROVIDED BY ELECTRICAL NOISE MEASUREMENTS

- The electrical noise is sensitive to the addition of extracellular solutions, such as dopamine, Calcium Chloride and Potassium Chloride. The effect is metastable, and it only last for about 10-30 minutes. With time the curve of power spectral density as function of frequency recovers its original shape. These effects are only observed below a frequency of 1 Hz. Fig. 40 shows an example of this behaviour.

- The DC level of the noise provides relevant information about cell death or cell detachment from the surface. The addition of a high dose of dopamine often causes some cell mortality. As cells detach from the surfaces the average noise DC level decreases with time. The best way to observe this effect is to perform the histogram analysis of time domain traces as shown in Fig. 41. When cells detach from the solid surface the total resistance (from the membrane) contributing to thermal noise decreases. The same phenomena can be monitored in the impedance. There is a movement of the relaxation frequency to higher values (see Fig. 27).

- Electrical stimulation of the C6 glial cells can induce a cooperative bioelectrical activity. After the application of the train of pulses some bursts of activity were measured. These activity bursts became synchronized after a period (~20 minutes) of random activity as shown in Fig. 34. Although C6 cells cannot generate action potentials, their response, which is chemically encoded, can be revealed by transients and oscillations of Ca^{2+} and other ions [47]. Calcium responses often spread to surrounding cells creating a calcium wave [50]. Random spikes of spontaneous calcium oscillations have been reported [50] as well as synchronized like operation [48].

Chapter 6

CONCLUSIONS

The main results can be summarized as follows:

- A support was designed to hold a variety of sensing devices and can be plugged into several measuring systems. This device holder allow keeping cells cultures alive over extended periods of time and allow the use of optical based techniques.

- Several types of sensing devices were developed and tested from simple microelectrode arrays on oxidized silicon. It was also shown that the transistor type of devices allows also bi-directional communication and were successful tested to induce bioelectrical activity. A set of typical signals is shown in Table I.

- Protocols for performing a number of electrical measurements were established and tested using cultured cells *in vitro*. The techniques are based on small-electrical signals. It was demonstrated that these measurements provide direct information about: (i) cell adhesion to the surfaces, (ii) cell health state and natural bioelectrical activity or upon chemical and electrical stimulus. A number of bioelectrical signals were recorded from cells kept alive over extended periods of time (weeks) on the top of the sensing devices.

Table V – Summary of electrical techniques and typical signal shapes that provide information about cells.

Sensing device	Technique	Protocol for measurements	Information provided	Typical signal shape
OFET Conductive or semi conductive electrodes	**Electrical** Small signal impedance	**Frequency** $[0 - 10^6 Hz]$	Cell adhesion Cell health state Changes in the conductivity of the surrounding electrolyte medium	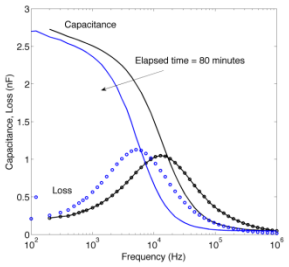
OFET Conductive or semi conductive electrodes	**Electrical** Noise based techniques	**Time dependence of the electrical noise**	Changes in the conductivity of the surrounding electrolyte medium	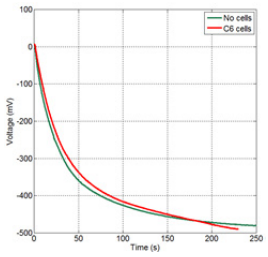
OFET Conductive or semi conductive electrodes	**Electrical** Noise based techniques	**Frequency** $[0 - 10^6 Hz]$	Transient effect caused by the addition of extracellular solution stimulus. Only noticeable below 1 Hz	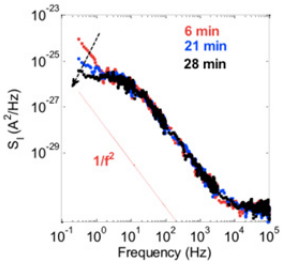
OFET Conductive or semi conductive electrodes	**Electrical** Noise based techniques	**Histogram**	Cell Health state	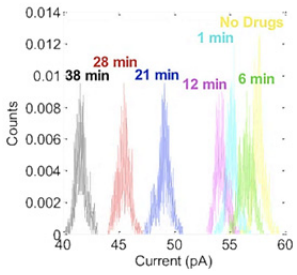
OFET Conductive or semi conductive electrodes	**Electrical** Noise based techniques	**Time dependence of the electrical noise**	Cell bioelectrical activity	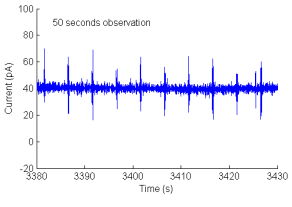

6.1 FUTURE WORK

In a future work some improvements or knowledge can be reached with the following steps:

- New extracellular chemical stimuli can be used in order to improve a library of signals based on simulated responses, as so the reaction of the same stimuli in new devices with the same or different cells type.

- Re-design the created support for sensing devices to be adapted to different devices configuration.

REFERENCES

[1] Berggren, M.; Richter-Dahlfors, A., *Organic Bioeletronics*. 2007, Advanced Materials, 19, p. 3201-3213, Ed. Wiley-VCH.

[2] Fromherz, P., *Neuroeletrocnic Interfacing: Semiconductor Chips with Ion Channels, Nerve Cells and Brain*, *Nanoelectronics and Information Technology*. 2003, p. 781-810, Ed. Rainer Waser, Ed. Wiley-VCH.

[3] Hierlemann, A., *Introduction to Silicon Process Technology*. Microtechnology and Microelectronics, s/d, (626-0001-00L). Retrieved, 08/07/2013, from the World Wide Web: http://www.bsse.ethz.ch/bel/education/lectures.

[4] Heeger, A.; MacDiarmid, A.; Shirakawa, H., *Conductive polymers*. Advanced information from The Nobel Prize in Chemistry, 2000. Retrieved, 08/07/2013, from the World Wide Web: http://www.nobelprize.org.

[5] Willner, I.; Katz, E., *Bioelectronics: From Theory to Applications*. Weinheim: Wiley-VCH Verlag GmbH & Co. KGaA. 2005. ISBN: 3-527-30690-0.

[6] Poghossian, A.; Ingebrandt, S.; Offenhäuser, A.; Schöning, M., *Field-effect devices for detecting cellular signals*. 2009, Seminars in Cell & Development Biology, 20, p. 41-48.

[7] Brittinger, M.; Fromhertz, P., *Field-effect transistor with recombinant potassium channels: fast and slow response by electrical and chemical interactions*. 2005, Applied Physics A, 81, p. 439-447.

[8] Ulbrich, M.; Fromherz, P., *Opening of K^+ channels by capacitive stimulation from silicon chip*. 2005, Applied Physics A, 81, p. 887-891.

[9] Schmidtner, M.; Fromherz, P., *Functional Na^+ Channels in Cell Adhesion probed by Transistor Recording*. 2006, Byophysical Journal, 90, p. 183-189.

[10] Vassanelli, S.; Fromherz, P., *Transistor Probes Local Potassium Conductances in the Adhesion Region of Cultured Rat Hippocampal Neurons*. 1999, The Journal of Neuroscience, 19, p. 6767-6773.

[11] Thedinga, E.; Bob, A.; Holst, H.; Keuer, A.; Drechsler, S.; Niendorf, R.; Baumann, W.; Freund, I.; Lehmann, M.; Ehret, R., *Online monitoring of cell metabolism for studing pharmacodynamics effects*. 2007, Toxicology and Applied Pharmacology, 220, 33-44.

[12] Cui, Y.; Zhong, Z.; Wang, D.; Wang, W.; Lieber, C., *High Performance Silicon Nanowire Fiel Effect Transistors*. Nano letters, 2003, 3(2), 149-152.

[13] Cheng, M.; Cuda, G.; Bunimovich, Y.; Gaspari, M.; Heath, J.; Hill, H.; Mirkin, C.; Nijdam, A.; Terracciano, R.; Thundat, T.; Ferrari, M., *Nanotechnologies for biomolecular detection and medical diagnostics.* 2006, Chemical Biology, 10, 11-19.

[14] Mazzatenta, A.; Giugliano, M.; Campidelli, S.; Gambazzi, L.; Businaro, L.; Markram, H.; Prato, M.; Ballerini, L., *Interfacing Neurons with Carbon Nanotubes: Electrical Signal Transfer and Synaptic Stimulation in Cultured Brain Circuits*. 2007, The Journal of Neuroscience, 27(26), 6931-6936.

[15] Spira, M.; Hai, A., *Multi-electrode array technologies for neuroscience and cardiology*. 2013, Nature Nanotechnology, vol.8, 83-94.

[16] Xie, C.; Lin, Z.; Hanson, L.; Cui, Y.; Cui, B., *Intracellular recording of action potencials by nanopilar electroporation*. 2012, Nature Nanotechnology, vol.7, 185-190.

[17] Veres, J., Ogier, S., Lloyd, G.; Leeuw, D., *Gate Insulators Field-Effect Transistors*. 2004, Chem. Mater., 16, 4543-4555.

[18] Kergoat, L.; Piro, B; Berggren, M; Horowitz, G.; Pham, M., *Advances in organic transistor-based biosensors: from organic electrochemical transistors to electrolyte-gated organic field-effect transistors.* 2012, Anal Bioanal Chem, 402, 1813-1826.

[19] Forrest, S., *The path to ubiquitous and low-cost organic electronic appliances on plastic.* 2004, Nature, vol. 428, 911-918.

[20] Berggren, M.; Nilsson, D.; Robinson, N., *Organic materials for printed electronics.* 2007, Nature Materials, vol.6, 3-5.

[21] Richardson-Burns, S.; Hendricks, J.; Foster, B.; Povlich, L.; Kim D.; Martin, D., *Polymerization of the conducting polymer poly(3,4-ethylenedioxythiophene) (PEDOT) around living neural cells.* 2007, Biomaterials, 28, p. 1539-1552.

[22] Abidian, M.; Corey, J.; Kipke, D.; Martin, D., *Conducting-Polymer Nanotubes Improve Electrical Properties, Mechanical Adhesion, Neural Attachment, and Neurite Outgrowth of Neural Electrodes.* 2010, Small, 6 (3), p. 421–429.

[23] Benfenati, V.; Toffanin S.; Bonetti, S.; Turatti, G.; Pistone, A.; Chiappalone, M.; Sagnella, A.; Stefani, A.; Generali, G.; Ruani, G.; Saguatti, D.; Zamboni, R.; Muccini, M., *A transparent organic transistor structure for bidirectional*

stimulation and recording of primary neurons. 2013, Nature Materials, vol.12, p. 672-680.

[24] Yang, S.; Kim, B.; Zadkhidov, A.; Taylor, P.; Lee, J.; Ober, C.; Lindau, M.; Malliaras, G., *Detection of transmitter release from single cells using conducting polymer microelectrodes.* 2011, Advanced Materials, NIH-PA Author Manuscript, 23 (24), p. 10.

[25] Tinti, R.; Sischka, F.; Morton, C., *Proposed System Solution for 1/f Noise Parameter Extraction*. Agilent Product Note 5989-9087EN, 2000. Retrieved, 08/07/2013, from the World Wide Web: http://www.agilent.com.

[26] Malmivuo, J.; Plonsey, R., *Bioelectromagnetism: Principles and applications of Bioelectric and Biomagnetic Field*. 1995, Oxford University Press, p. 56-62.

[27] Green, R.; Lovell, N.; Wallace, G.; Poole-Warren, L., *Conducting polymers for neural interfaces: Challenges in developing an effective long-term implant.* 2008, Biomaterials, 29, p. 3393-3399.

[28] Bettinger, C.; Bao, Z., *Biomaterials-based organic electronic devices.* 2010, Wiley Interscience, 59, p. 563-567.

[29] Tarabella, G.; Santato, C.; Yang, S.; Iannotta, S.; Malliaras, G.; Cicoira, F., *Effect of the gate electrode on the response of organic electrochemical transistors.* 2010, Applied Physics Letters, AIP Publishing LLC, 97, 123304.

[30] Yang, S., Kim, B., Zakhidov, A., Lee, J., Ober, C., Lindau, M., Malliaras, G., *Detection of transmitter release from single cells using conducting Polymer Microelectrodes*. Advanced Materials, 2011, 23, p. 184-188.

[31] Khodagholy, D.; Rivnay, J.; Sessolo, M.; Gurfinkel, M.; Leleux, P.; Jimison, L.; Stavrinidou, E.; Herve, T.; Sanaur, S.; Ownes, R.; Malliaras, G., *High transcondutance organic electrochemical transistors*. 2013, Nature Comunications, 4, article number 2133, p. 1-6

[32] Hoehne, F., *Neuro-Transistors.* Course 5: Semiconductors and Nanostructures. JASS 2005 St. Petersburg. 6 p.

[33] Seeley, R.; Stephens, T.; Tate, P. *Anatomia & Fisiologia*. 2005. Lusociência, pp. 376-377; 388-389.

[34] Berggren, M.; Forchheimer, R.; Bobacka, J.; Svensson, P; Nilsson, D.; Larsson, O.; Ivaska, A., *PEDOT:PSS-Based Electrochemical Transistors for Ion-to-Electron Transduction and Sensor Signal Amplification. Organic Semiconductors*

in Sensor Applications. 2008, Material Science vol.107, 2008, p. 263-280, Ed. Springer.

[35] Cramer, T.; Kyndiah, A.; Murgia, M.; Leonardi, F.; Casalini, S. *et al*., *Double layer capacitance measured by organic field effect transistor operated in water.* 2012, Applied Physics Letters, 100, 143312.

[36] Cramer, T.; Chelli, B.; Murgia, M.; Barbalinardo, M.; Bystrenova, E.; Leeuw, D.; Biscarini, F., *Organic ultra-thin film transistors with a liquid gate for extracellular stimulation and recording of electric activity of stem cell-derived neuronal networks.* 2013, PCCP, p. 3-12, RSC Publishing.

[37] Bier, M., *How to evaluate the electric noise in a cell membrane?*. 2006, Acta Physica Polonica B, n.º5, vol.37, p. 1409-1424.

[38] http://www.lgcstandards-atcc.org/. Retrieved, 28/07/2013, from the World Wide Web: http://www.lgcstandards-atcc.org/en/Global/Products/3/1/1/D/CCL-107.aspx or http://www.lgcstandards-atcc.org/products/all/CCL-131.aspx.

[39] Ehret, R.; Baumann, W.; Brischwein, M.; Schwinde, A.; Wolf, B. *On-line control of cellular adhesion with impedance measurements using interdigitated electrode structures*. May 1998, Medical & Biological Engineering & Computing, vol. 36, pp. 365-370.

[40] Ehret, R.; Baumann, W.; Brischwein, M.; Schwinde, A.; Stegbauer, K.; Wolf, B., *Monitoring of cellular behaviour by impedance measurements on interdigitated electrode structures*. 1997, Biosensors & Bioelectronics, vol. 12, pp. 29-41.

[41] Wegener, J.; Keese, C. R.; Giaever, I., *Electric cell-substrate impedance sensing (ECIS) as a noninvasive means to monitor the kinetics of cell spreading to artificial surfaces*, August 2000, Exp Cell Res, vol. 259, pp. 158-66.

[42] Yang, L.; Li, Y.; Griffis, C. L.;. Johnson, M. G., *Interdigitated microelectrode (IME) impedance sensor for the detection of viable Salmonella typhimurium,* Biosens Bioelectron*,* May 2004, vol. 19, pp. 1139-47.

[43] Giaever I.; Keese, C. R., *A Morphological Biosensor for Mammalian-Cells,* Nature*,* December 1993, vol. 366, pp. 591-592.

[44] Arndt, S.; Seebach, J.; Psathaki, K.; Galla, H. J.; Wegener, J., *Bioelectrical impedance assay to monitor changes in cell shape during apoptosis*, Biosensors & Bioelectronics, January 2004, vol. 19, pp. 583-594.

[45] Madrid, R. E.; Felice, C. J.; Valentinuzzi, M. E., *Automatic on-line analyser of microbial growth using simultaneous measurements of impedance and turbidity*, Med Biol Eng Comput, November 1999, vol. 37, pp. 789-93.

[46] Luong, J. H.; Habibi-Rezaei, M.; Meghrous, J.; Xiao, C.; Male, K. B.; Kamen, A., *Monitoring motility, spreading, and mortality of adherent insect cells using an impedance sensor*, Anal Chem, April 2001., vol. 73, pp. 1844-8.

[47] Charles, A. C.; Naus, C. C.; Zhu, D.; Kidder, G. M.; Dirksen, E. R.; Sanderson, M. J., *Intercellular calcium signaling via gap junctions in glioma cells*, J Cell Biol, Jul 1992, vol. 118, pp. 195-201.

[48] Steinbeck, J. A.; Henke, N.; Opatz, J.; Gruszczynska-Biegala, J.; Schneider, L.; Theiss, S.; Hamacher, N.; Steinfarz, B.; Golz, S.; Brustle, O.; Kuznicki, J.; Methner, A., *Store-operated calcium entry modulates neuronal network activity in a model of chronic epilepsy*, Exp Neurol, Dec 2011, vol. 232, pp. 185-94.

[49] Wagenaar, D. A.; Pine, J.; Potter, S. M., *An extremely rich repertoire of bursting patterns during the development of cortical cultures*, Bmc Neuroscience, Feb 2006, vol. 7.

[50] Wu, X.; Pan, L.; Liu, Y.; Jiang, P.; Lee, I.; Drevensek-Olenik, I.; Zhang, X.; Xu, J., *Cell-cell communication induces random spikes of spontaneous calcium oscillations in multi-BV-2 microglial cells*, Biochem Biophys Res Commun, Feb 2013, vol. 431, pp. 664-9.

[51] Auld, D.S., *Glial Cells and Neurotransmission: An Inclusive View of Synaptic Function*, 2003, **40**, 389-400

[52] Barrs, B.A., *New Roles for Glia*, The Journal of Neuroscience, 1991, **11(12)**: 3685-3694

[53] Verkharatsy, A.; Kettenmann, H., *Calcium signalling in glial cells.* Trends Neurosci, 1996, **19**, 346-352

[54] Verkhratsky, A.; Steinhauser, C., *Ion channels in glial cells.* Brain Research Reviews, 1999 **32**, 380-412.

[55] Eickhorn, R.; Weirich,J.; Hornung,D.; Antoni, H., *Use dependence of sodium current inhibition by tetrodotoxin in rat cardiac muscle: influence of channel state.* Pflügers Arch, 1990, **416**:398 – 405.

[56] North, R.A., *The Calcium-dependent slow after-hyperpolarization in in myenteric plexus neurons with tetrodotoxin-resistant action potentials,* 1973, 709-711.

[57] O'Connor, E. R.; Kimelberg, H.K., *Role of Calcium in Astrocyte Volume Regulaton and in the Release of Ion and Amino Acids.* The Journal of Neuroscience, 1993, **13(6)**: 2638-2650

[58] Purves, D.; Augustine, G.J.; Fitzpatrick, D.; Hall, W.C.; LaMantia, A.; McNamara, J.O.; Williams, S.M., *NEUROSCIENCE*: Third Edition, Sinauer Associates, Inc., 2004.

[59] Eickhorn, R.; Weirich,J.; Hornung,D.; Antoni, H., *Use dependence of sodium current inhibition by tetrodotoxin in rat cardiac muscle: influence of channel state.* Pflügers Arch, 1990, **416**:398 – 405;

[60] North, R.A., *The Calcium-dependent slow after-hyperpolarization in in myenteric plexus neurons with tetrodotoxin-resistant action potentials*. 1973, 709-711.

[61] Moura, L.; Darwazeh, I.; *Introduction to Linear Circuit Analysis and Modelling: From DC to RF.* Oxford: Elsevier. 2005. ISBN: 07506 59327.

[62] Wang, J.; Wu, C.; Hu, N.; Zhou, J. Du, L.; Wang, P., *Microfabricated Electrochemical Cell-Based Biosensors for Analysis of Living Cells* In Vitro. Biosensors, 2012, vol.2, pp.127-170.